LAMELLAR COMPOSITES FORMED BY SPUTTER DEPOSITION; PROPERTIES AND POTENTIAL APPLICATION TO TURBINE BLADES

R. A. Busch, et al

Battelle Pacific Northwest Laboratories

Prepared for:

Air Force Office of Scientific Research

July 1975

UNCLASSIFIED

SECURITY CLASSIFICATION OF THIS PAGE *(When Date Entered)*

REPORT DOCUMENTATION PAGE

READ INSTRUCTIONS BEFORE COMPLETING FORM

1. REPORT NUMBER: AFOSR - TR - 76 - 0013
2. GOVT ACCESSION NO
3. RECIPIENT'S CATALOG NUMBER

4. TITLE *(and Subtitle)*: LAMELLAR COMPOSITES FORMED BY SPUTTER DEPOSITION; PROPERTIES AND POTENTIAL APPLICATION TO TURBINE BLADES

5. TYPE OF REPORT & PERIOD COVERED: INTERIM 1 May 1974 to 30 June 1975

6. PERFORMING ORG. REPORT NUMBER

7. AUTHOR(s)
R BUSCH
J W PATTEN

8. CONTRACT OR GRANT NUMBER(s): F44620-73-C-0071

9. PERFORMING ORGANIZATION NAME AND ADDRESS
BATTELLE, PACIFIC NORTHWEST LABORATORIES
BATTELLE BOULEVARD, PO BOX 999
RICHLAND, WASHINGTON 99352

10. PROGRAM ELEMENT, PROJECT, TASK AREA & WORK UNIT NUMBERS: 681307, 9782-05, 61102F

11. CONTROLLING OFFICE NAME AND ADDRESS
AIR FORCE OFFICE OF SCIENTIFIC RESEARCH/NA
BUILDING 410
BOLLING AIR FORCE BASE, D C 20332

12. REPORT DATE: July 1975

13. NUMBER OF PAGES: 88

14. MONITORING AGENCY NAME & ADDRESS *(if different from Controlling Office)*

15. SECURITY CLASS. *(of this report)*: UNCLASSIFIED

15a. DECLASSIFICATION DOWNGRADING SCHEDULE

16. DISTRIBUTION STATEMENT *(of this Report)*

Approved for public release; distribution unlimited.

17. DISTRIBUTION STATEMENT *(of the abstract entered in Block 20, if different from Report)*

18. SUPPLEMENTARY NOTES

19. KEY WORDS *(Continue on reverse side if necessary and identify by block number)*

LAMELLAR COMPOSITES
SPUTTER DEPOSITION
COPPER-MOLYBDENUM
BERYLLIUM-TITANIUM
NICKEL-ALUMINUM
TITANIUM-ALUMINUM
BERYLLIUM-ALUMINUM

20. ABSTRACT *(Continue on reverse side if necessary and identify by block number)*

Data and results from the second year's evaluation of two types of lamellar composites is presented and discussed.

i

DD FORM 1 JAN 73 1473 EDITION OF 1 NOV 65 IS OBSOLETE

UNCLASSIFIED

A Research Report

Lamellar Composites Formed by Sputter Deposition; Properties and Potential Application to Turbine Blades

Annual Technical Report: July 1975

R. A. Busch and J. W. Patten

Sponsored by Advanced Research Projects Agency

Contract No. F44620-73-C-1071
Modification P00003, July 8, 1974
ARPA Order No. 2482-2
Program Code No. 5D10

Battelle
Pacific Northwest Laboratories

88

LEGAL NOTICE

This report was prepared by Battelle as an account of sponsored research activities. Neither Sponsor nor Battelle nor any person acting on behalf of either:

a. Makes any warranty or representation, express or implied, with respect to the accuracy, completeness, or usefulness of the information contained in this report, or that the use of any information, apparatus, method, or process disclosed in this report may not infringe privately owned rights; or

b. Assumes any liabilities with respect to the use of, or for damages resulting from the use of, any information, apparatus, method, or process disclosed in this report.

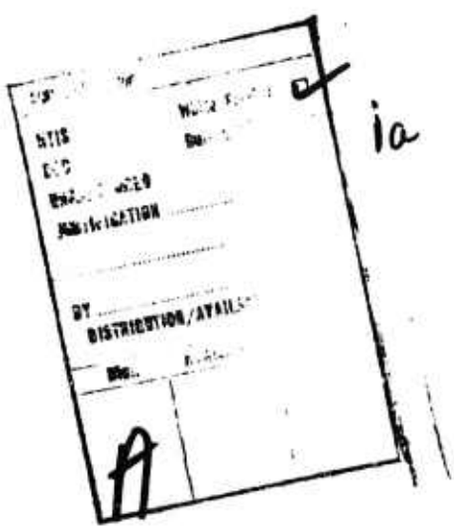

LAMELLAR COMPOSITES FORMED BY SPUTTER DEPOSITION; PROPERTIES AND POTENTIAL APPLICATION TO TURBINE BLADES

Annual Technical Report

July 1975

Sponsored by Advanced Research Projects Agency

Contract No. F44620-73-C-0071
Modification P00003, July 8, 1974
ARPA Order No. 2482-2
Program Code No. 5D10

Principal Investigator
H. R. Gardner
509-942-2305

Program Managers
R. A. Busch
509-942-2685

J. W. Patten
509-942-2603

Contract Technical Monitor
Wm. Walker

Effective Date
May 1, 1973

Contract Expiration Date
June 30, 1975

Amount of Contract
$342,631

BATTELLE
PACIFIC NORTHWEST LABORATORIES
RICHLAND, WASHINGTON 99352

CONTENTS

LIST OF FIGURES

LIST OF FIGURES (contd)

LIST OF TABLES

INTRODUCTION

This report presents the results of the research done during the second year or Phase II of an investigation of the properties and behavior of lamellar composites formed by sputter deposition. The overall objective of the work was to develop lamellar composite technology that could be beneficially applied to engineering problems considered relevant to the Department of Defense and related agencies.

Briefly, lamellar composites formed by sputter deposition consist of alternate layers of dissimilar elements and/or compounds. Selection of layer thickness and component can be made to establish the validity of theoretical considerations and so provide a scientific basis for design of engineering materials. Two approaches have been investigated in parallel in Phases I and II of the contract. Both were expected to result in yield strengths on the order of 1% or more of the modulus of the composite material. The thin-layered approach, with $\sim$50 Å thick layers, was expected to derive its strengthening from interface effects between layers and the small thickness of the layers. The compound-forming approach, with $\sim$2000 Å thick layers, was expected to derive its strengthening from the bulk properties of the components and their reaction products.

In general, the Phase II objectives were to expand property and behavior data on the composites to provide the technology base necessary for consideration of engineering applications. A secondary objective was to seek information from DOD agencies on potential applications of the technology.

SUMMARY

TECHNICAL PROBLEM

The objective of the program was to develop new composites which display properties more desirable than the properties of either component material by itself. Mechanical properties and their thermal stability were of primary interest for assessment of usefulness in engineering applications.

Thin-Layered Systems

Koehler[1] has proposed the design of a strong solid composed of alternate layers of materials with high and low elastic constants. He expects yield strengths on the order of 1% of the elastic modulus if layers are thin enough ($\sim$200 Å) to prevent the operation of Frank-Reed sources. In addition, since up to 20 Å of a pure metal may assume the crystal structure of another metal upon which it has been deposited,[2-4] i.e., pseudomorphic or epitaxial growth, the interface region would be very highly stressed in the manner of Guinier-Preston zones or boundaries of other coherent precipitates.

The object of the thin-layered system program is to fabricate lamellar composites with layers less than 200 Å thick. These layers would consist of two metals mutually insoluble in the solid state, with different crystal structures and with widely different elastic moduli and coefficients of thermal expansion. Contributions to a high level of internal stress should be realized from lattice distortion produced by pseudomorphic layers, fine grain size, high internal stress levels achievable in pure sputtered materials, and property mismatch. It is not expected that Frank-Reed sources will operate within a given layer; therefore, dislocations should be very difficult to generate. The long-range nature of the dislocation barriers (layer interfaces) together with the need to preserve Burgers vector in moving across an interface should also make dislocation movement very difficult. Vacancy diffusion to the interfaces and subsequent defect movement should provide the only deformation mechanism.

Compound-Forming Systems

Compound-forming systems do not depend on the small dimensions of the layers for their properties. The elements or compounds forming the layers are selected for their individual properties and their compatibility with each other. The reinforcing layer consists of a high elastic modulus material such as an oxide, carbide or intermetallic compound; the other layer is a metal with a reasonable degree of plasticity. These composites could function similarly to existing composite materials in that the metal would protect, orient, and transfer load to the reinforcing layer. They would be

expected to achieve higher strengths than existing composites due to the strong bonding between layers. They may, however, suffer the drawback of a potential continuous crack path in the brittle reinforcing layer.

GENERAL METHODOLOGY

The general approach was experimental. Tensile testing and microhardness techniques were used to study mechanical properties as a function of relative and absolute laminate layer thickness, substrate temperature during deposition, and heat treatment temperature after deposition. In addition such techniques as x-ray diffraction, scanning electron microscopy, calorimetry, and resistivity measurements were used to gain insight into structure, fracture behavior, and other composite characteristics as a function of time and temperature.

Depositions on large cylindrical substrates were performed to provide tensile samples and additional material for metallurgical characterization.

Information was sought from the DOD and related agencies on potential applications of the sputter-deposited lamellar composite technology.

TECHNICAL RESULTS

Thin-Layered Systems

Phase I -- It was determined that the thin laminate structure provided a very effective new strengthening mechanism with excellent thermal stability and retention of mechanical properties to at least 0.6 of the absolute melting point of the lowest melting component. Deposits sputtered at temperatures below 100°C were very high integrity, highly strained layered structures with distinct and continuous alternating layers of Cu and Mo. Each of these layers were 50 to 100 Å thick and were composed of equiaxed grains 50 to 100 Å in diameter. Total composite thicknesses produced ranged up to 0.076 cm (0.030 in.), with an area of 800 cm^2. The composites were heavily textured with Cu (111) and Mo (110) planes oriented parallel to the layer planes. Pronounced peak splitting was also observed in x-ray diffraction patterns.

Room temperature hardness of as-deposited samples was as high as 717 DPH, which is much higher than that observed in either pure Cu or pure Mo. Calculation of strength based on hardness indicates that a measured hardness of 669 DPH corresponds approximately to an ultimate tensile strength of 18,100 kg/cm^2 (258,000 lb/in.^{2}). Therefore, at room temperature, the Cu-Mo laminate structure is much stronger than either pure Cu or pure Mo and is roughly three times stronger than expected by the rule of mixtures. Tensile testing to support the strength calculations based on hardness data met with only limited success since all fractures were brittle and occurred at low loads, precluding any measurement of σ_μ. The composite modulus was found to be 1.52 x 10^6 kg/cm^2 (21.7 x 10^6 lb/in.^{2}). This was lower than the 2.35 x 10^6 kg/cm^2 expected from the rule of mixtures and was possibly the result of microcracking occurring during pretest fixturing. The calculated ultimate strength (σ_μ) of 18,100 kg/cm^2 (258,000 lb/in.^{2}), however, is approximately 0.77% of the modulus expected by the rule of mixtures, and 1.18% of the observed modulus. This value is in excess of the 1% of modulus value predicted by Koehler.(1)

With respect to the influence of temperature, the layered structure withstood a heat treatment of 4 hr at 500°C but broke down by spheroidization of the Mo after 2 hr at 750°C. The spheroidized structure after this heat treatment consisted of 860 Å diameter Mo spheres in a twinned Cu matrix. The Mo spheres grew in diameter with increasing time at temperature with 3000 Å diameter Mo spheres being observed after 4 hr at 1000°C. Hardness decreased with heat treatment above 650°C, a possible indication of the onset of Mo spheroidization. Room temperature hardness of a sample spheroidized by heat treatment at 1000°C for 4 hr, however, was still greater than the values observed for as-rolled Mo bar stock. In addition, the calculated room temperature ultimate strength of this sample was 8800 kg/cm^2 (125,000 lb/in.^{2}). This is approximately 1055 kg/cm^2 (15,000 lb/in.^{2}) higher than is observed for Mo, almost twice the maximum observed for pure Cu, and 1.4 times the value predicted by the rule of mixtures.

Calculations based on elevated temperature hardness data indicated that although above 600°C pure Mo is stronger than the Cu-Mo laminate, the Cu-Mo laminate exceeds the rule-of-mixtures predicted strength below 788°C and is nearly equal to it at 987°C.

Phase II -- Characterization of the lamellar composites formed in the Phase I work continued. Measured ultimate tensile strengths obtained from samples heat treated at 1000°C for 4 hr were slightly higher than the 8800 kg/cm^2 (125,000 lb/in.^{2}) calculated from hardness data. It was concluded, therefore, that the method used to calculate σ_μ from hardness in Phase I was generally conservative and that actual ultimate strengths would be higher than calculated values. Scanning electron microscopy of fracture surfaces revealed typical cleavage fractures for composite in the as-sputtered and heat-treated at 550°C conditions. Fracture in composite heat treated at 982°C followed the Mo sphere-Cu matrix boundaries.

X-ray diffraction examination of material deposited at temperatures of 400 to 450°C revealed that the Mo layers were heavily textured with Mo (110) planes oriented parallel to the layer planes (or deposit-substrate interface). The Cu layers were slightly textured with Cu (111) planes oriented parallel to the layer planes, corresponding to the recrystallization texture for sputter-deposited Cu.

Additional data on the spheroidization caused by heat treatment indicated that for 1 hr at 650°C or above, spheroidization was produced. Cu and Mo diffusion with a component perpendicular to the layer planes was responsible for the onset of Mo spheroidization and resulting breakdown of the layered structure with the later stages of Mo sphere coarsening proceeding, at least in part, by coalescence.

Activation energies, based on hardness and resistivity measurements from -196 to 982°C, indicated that there were three possible stages for the structural changes occurring during heat treatment at any given temperature. The first stage, associated with an activation energy of 9.6 kcal/mole, was thought to be due to vacancy migration to sinks. The second stage, associated with an activation energy of 10 to 22 kcal/mole, was thought to be

due to grain boundary or interface diffusion of Cu and Mo and was responsible for layer breakdown by formation of Mo spheres. It is possible, however, that the first stage also contributes to layer breakdown and thus it may not be appropriate to differentiate between the first and second stages. The third stage, associated with an activation energy of 70 kcal/mole, was thought to be due either to Mo diffusion through the Cu matrix or to Mo sphere coalescence and was responsible for sphere coarsening.

Additional information on the peak splitting observed in as-sputtered composite produced at temperatures less than 700°C, indicated that this phenomenon was not attributable to lattice strain induced by differences in thermal contraction on cooling from the sputtering temperature, or the occurrence of fcc Mo or other nonequilibrium structures. Furthermore, peak splitting was not observed in samples heat treated at sufficiently high temperatures. It is hypothesized that the observed peak splitting was a result of strains from crystallographically related growth of the Cu and Mo layers with possible contributions from strains induced by solid solution formation during sputter deposition. The nature of these strains is not clear. However, the x-ray diffraction data indicated that they were very short-range strains.

Compound-Forming Systems

Phase I -- Lamellar composites of alternate layers of titanium and beryllium-titanium (nominally corresponding to $TiBe_{12}$) formed by sputter deposition were found to have the potential for high strength. Composites were formed with titanium layers ranging in thickness from 0.09 to 0.17 μm and $TiBe_{12}$ compound layers ranging from 0.014 to 0.06 μm. Total composite thickness deposited ranged up to 0.025 cm (0.010 in.) with an area of 800 cm^2. It was found that the intermetallic compound was formed during deposition at a substrate temperature of 500°C and that the lamellar structure was stable up to 900°C, but broke down into a nonplanar geometry at higher temperatures.

Tensile testing of the composites was limited by premature failure at strains of less than 10^{-4}. The elastic moduli were 9 to 23% greater than

that of titanium, however no correlation with the relative compound or repeating layer (compound plus titanium) thickness was observed. The observed tensile strengths were in the 2.0 to 5.3 x 10^3 kg/cm^2 (29 to 76,000 lb/$in.^2$) range.

Bend test results revealed the following effects of the repeating and relative compound layer thickness:

a. At equal strain, higher strengths were observed with smaller repeating layer thickness and/or higher relative compound layer thickness.

b. A smaller relative compound layer thickness permitted greater plastic strain before fracture, and thus produced the highest observed strengths.

It was concluded that the lamellar composites had demonstrated the potential for high strength. The most profitable area for further investigation appeared to be that of smaller repeating layer thickness, and smaller proportions of the relative intermetallic compound.

Phase II -- The mechanical properties of lamellar composites formed by high-rate sputter deposition were determined, and an attempt was made to correlate the results with the characteristics of the lamellar structure. The composite alloy systems investigated were: titanium-titanium beryllide, aluminum-nickel aluminide, aluminum-titanium aluminide, and aluminum-beryllium. Typical lamellar thickness characteristics were: reinforced metal layers 0.5 to 1.0 micron, reinforcing layer 0.05 to 0.25 micron, total thickness 0.5 mm. The composites were deposited on 700 cm^2 copper substrates at rates of 1 to 2 microns/min. The lamellar structures were obtained by depositing from two semicylindrical targets onto a rotating cylindrical substrate. The layer thicknesses were controlled by the voltages applied to the individual targets and the rotation rate of the substrate.

In the titanium-titanium beryllide system, the observed flow stress at a given strain varied in the expected manner with the degree of reinforcement. The fracture stress, however, was greatest in the composites with smaller degrees of reinforcement, due to their greater plastic strain and

the high strain hardening rate. Tensile strengths of 100 ksi and extreme fiber stresses in bending of 500 ksi were observed with less than 10% reinforcement.

The properties of the aluminum-based systems were not consistently dependent on the degree of reinforcement. However, reinforcement was obtained in all cases, as shown by elastic moduli 30 to 60% greater than pure aluminum. Strengths of 40 to 65 ksi in tension and 135 to 280 ksi (extreme fiber) in bending were observed. Total strain (elastic + plastic) to fracture was of the order of 0.5%.

The layer structure was stable to temperatures in excess of 0.6 of the absolute melting point in all systems investigated. The titanium-titanium beryllide system showed spheroidization at 0.7 Tm, while the aluminum-based systems were stable at this homologous temperature. The aluminum-nickel aluminide system exhibited extensive breakup and instability of the intermetallic layers in the necked region when deformed at 0.6 Tm. At this temperature, the aluminum-titanium aluminide and aluminum-beryllium systems were about three times as strong, did not exhibit necking, and retained their continuous layer structure during deformation.

All systems exhibited thorough bonding of the lamellar structure in all conditions examined, including heat treatments and bend fractures.

The small fracture strains at room temperature, together with the high strengths observed at testing temperatures of 0.6 Tm, indicate the potential utility of this class of materials in high temperature applications such as gas turbine blading.

THIN-LAYERED SYSTEMS

MATERIALS AND PROCEDURES

Only evaluation techniques not discussed in previous reports[5,6] are described in the following.

Density

Densities of specimens from deposit OTLC-2 were measured in a temperature compensated displacement device with reference to standards of known density using techniques similar to those developed by Nelson.[7,8] Densities were judged to be accurate within 0.01 g/cm^3. The density data were useful only as a rough indicator of deposit porosity and as verification of the amount of Cu and Mo in the deposits.

Scanning Electron Microscopy (SEM)

Fracture surfaces were examined in a scanning electron microscope (SEM) to determine mode of fracture and its relation to composite structure.

Resistivity

Resistivity measurements were made in a Battelle-Northwest designed and constructed apparatus using a four-probe technique and a digital data acquisition and analysis system. In specimen preparation, copper substrates were machined away from the deposits on a milling machine with the final copper removal being accomplished with 600-grit abrasive paper. Resistivity samples were then cut from the free-standing deposits by electrical discharge machining. Sample size was typically 2.54 cm long, 0.254 cm wide, and the thickness of the deposit (0.023 to 0.076 cm). Most resistivity samples were taken from deposit OTLC-2 in order to correlate resistivity data with transmission electron microscopy (TEM) data. Resistivity leads of high purity platinum were spot welded to the samples as was a Type R (platinum-13% rhodium versus platinum) thermocouple. Sample, resistivity leads, and thermocouple were mounted on a quartz rod and room-temperature resistivity was measured. The assembly was then plunged into a fluidized bed consisting of ZrO_2 powder in a quartz tube with a continuous argon flow through a porous quartz tube bottom. The bed was maintained at temperatures up to 1000°C by an automatically controlled and monitored tube furnace. Resistance at constant temperature was measured every 2 sec with a recording digital voltmeter as a function of time at temperature until resistance had ceased to change

rapidly. The sample was then removed from the fluidized bed and allowed to cool to room temperature. Sample size was measured with a micrometer and an optical comparator and resistivity was calculated. The resistivity was measured again at room temperature, in liquid nitrogen, and a third time at room temperature. Errors in sample dimension measurement may have resulted in absolute resistivity errors on the order of 15%; however, it is felt that resistance measurements were accurate within 1%. The resistivity change data were used to calculate activation energies for the processes responsible for structural changes that occurred as a function of time and temperature.

RESULTS AND DISCUSSION

X-Ray Diffraction

Line Broadening

Analysis of line broadening in x-ray diffractometer patterns of the deposits indicated that the broadening was caused by the extremely thin layers or small grain size rather than by lattice strain. Calculation of layer thickness (or grain size) from the line broadening resulted in a range of 73 to 119 Å which was in good agreement with the results of TEM (reported in a later section).

Peak Splitting

As reported previously[6] a peak splitting phenomena was observed which was felt to be related to distortions in the Mo (110) and Cu (111) interplanar spacings. It was demonstrated that the peak splitting was not caused by instrumental problems in the diffractometer. In the present work several phenomena were investigated as potential structural sources of the peak splitting. These included lattice strain induced during cooling after deposition; the periodicity of the layered structure; the presence of fcc Mo; the formation of substitutional solid solutions; and accommodation strains resulting from crystallographically related growth of the Cu and Mo layers. Each is treated in the following discussion.

Lattice Strain Induced During Cooling After Deposition. One possible cause for the peak-splitting phenomenon was lattice strain induced by differences in coefficient of thermal expansion on cooling. At first glance this does not seem a likely cause as the difference in thermal expansion coefficients between Cu and Mo is approximately 11.5×10^{-6}/°C and deposits were cooled less than 100°C from the deposition temperature to room temperature. Thermal contraction, therefore, would be on the order of 11.5×10^{-4} or 0.115%. This analysis, however, does not take into account that the surface of a sputtered deposit during deposition may be at a very high temperature. The energy distributions of sputtered atoms are usually peaked at a few eV which corresponds to adatom temperatures near 30,000°K.[9-11] In order to investigate the possibility that residual cooling stress was responsible for lattice distortion, it was reasoned that heating a sample should relieve some of these stresses, cause a relaxation in lattice strain, and reduce the 2θ separation in split Mo (110) and Cu (111) peaks. Accordingly, a sample from deposit 0TLC-2 was mounted in a specially designed integrally heated x-ray diffractometer holder and examined at 28, 125, and 225°C. The recorded diffraction pattern from $2\theta = 40°$ to $2\theta = 48°$ and the $\Delta 2\theta$ separation of peaks is presented in Figure 1. The essentially negligible change in $\Delta 2\theta$ with increasing temperature indicates that residual cooling stresses were not the source of the peak splitting. These data also indicate that the structure responsible for the extra peaks expanded at the same rate as the Cu and Mo layers.

Periodicity of the Layered Structure. The possibility of the periodicity of the layered structure as a cause of the peak splitting was investigated by comparison of x-ray diffraction patterns from the as-sputtered and 500°C and 750°C heat-treated conditions. The data taken after a 3-hr, 500°C heat treatment are presented in Figure 2. The Cu (111) peak splitting was not altered by heat treatment. The Mo (110) region, however, acquired another reflection corresponding to an interplanar spacing, d_{hkl}, larger than that for equilibrium Mo (110). No similar reflection was observed from as-sputtered samples. Further, the $\Delta 2\theta$ values for the second to

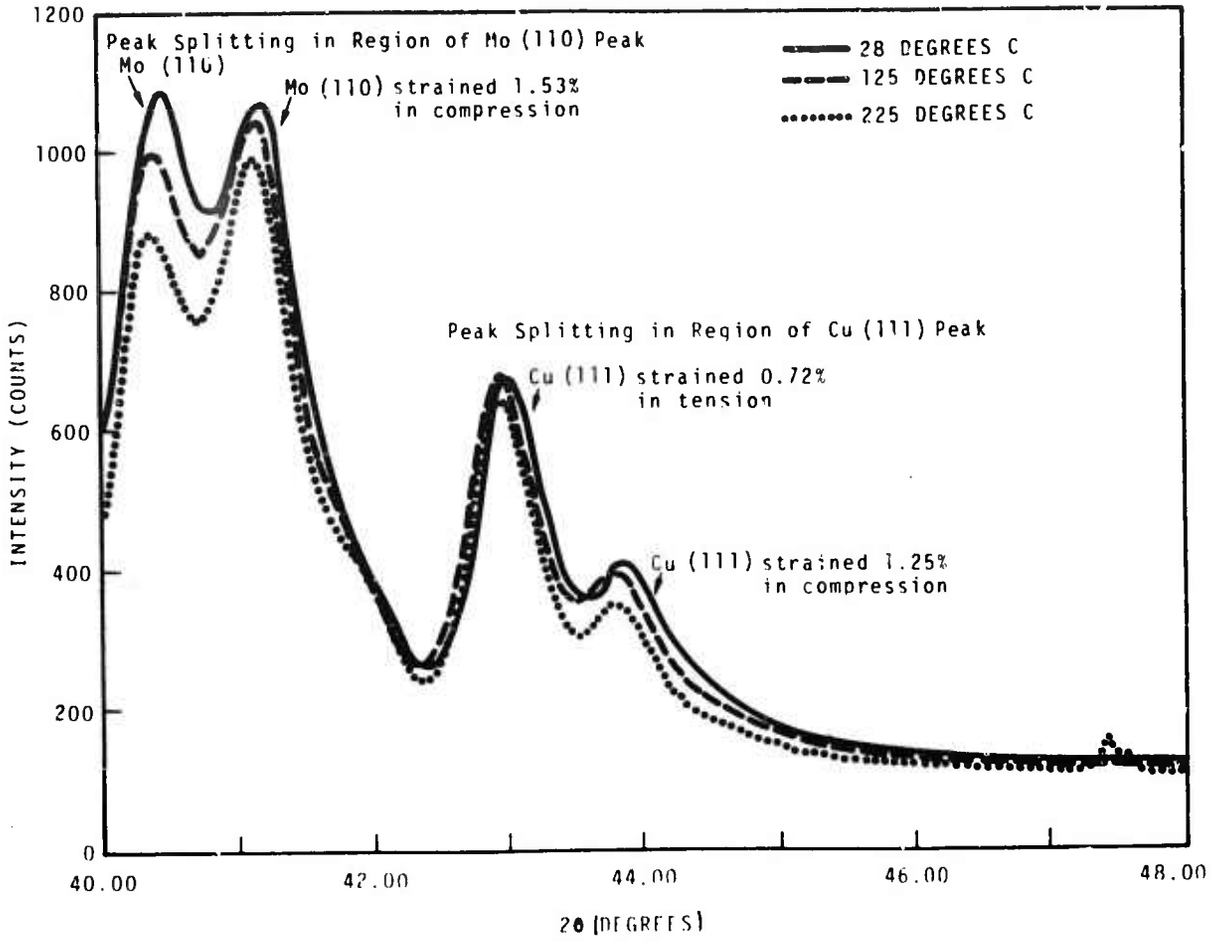

FIGURE 1. Influence of Sample Temperature on Peak Separation for Deposit OTLC-2 in the As-Sputtered Condition. (Absolute 2θ values may not be accurate.)

Temperature (°C)	Mo (110) (Δ2θ)	Cu (111) (Δ2θ)
28	0.72	0.84
125	0.76	0.90
225	0.76	0.83

third Mo (110) peaks increased from the as-sputtered values (Figure 1) indicating that heat treatment at 500°C for 3 hr decreased the interplanar spacing for this reflection. The change in relative peak heights observed near Mo (110) may indicate that the largest interplanar spacing structure

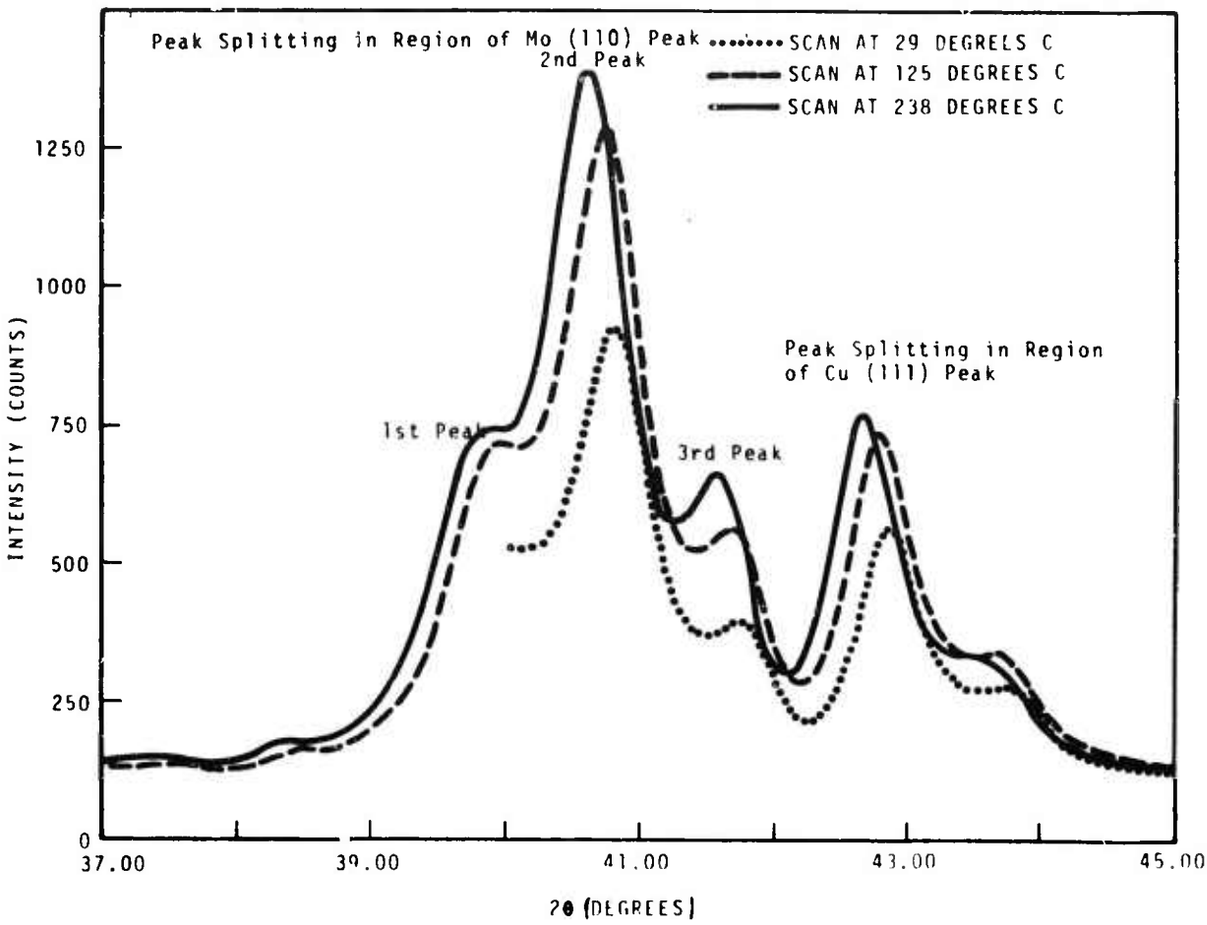

FIGURE 2. Influence of Sample Temperature on Peak Separation for Deposit OTLC-2, Heat Treated at 500°C for 3 Hr

Temperature (°C)	Mo (110) (Δ2θ) 1st to 2nd Peaks	2nd to 3rd Peaks	Cu (111) (Δ2θ)
28	Not measured	0.97	0.92
125	0.59	0.96	0.92
225	0.60	0.93	0.87

(first peak) formed at the expense of the shortest interplanar spacing structure (third peak). The largest interplanar spacing near Cu (111) also seemed to be favored by the heat treatment.

Since the layered structure persisted after the 500°C heat treatment, the resultant changes in peak location and emergence of a new peak during the heat treatment, then, indicate that the peak splitting phenomenon is not a diffraction effect produced by the periodicity of the layered structure.

Presence of fcc Mo. The possibility of peak splitting being caused by the presence of the nonequilibrium fcc Mo structure was considered. Lattice effects related to the epitaxial or pseudormorphic growth of nonequilibrium phases on a substrate surface have been reported by Jesser and Mathews[2-4] and vapor-deposited fcc Mo with a lattice parameter of $a_o = 4.16$ Å has been reported by Aggarwal and Goswami.[12] At this point because of the relative obscurity of data on fcc Mo, some digression for a discussion of the information obtained from the literature is considered appropriate. The previously mentioned lattice parameter, $a_o = 4.16$ Å, results in the fcc Mo interplanar spacings and 2θ Bragg reflection values listed in Table 1. Other investigators have also reported fcc Mo obtained by sputter deposition[13] and evaporation[14-16] with a lattice parameter of approximately $a_o = 4.19$ Å.

TABLE 1. Calculated Interplanar Spacings, d_{hkl} for fcc Mo Based on $a_o = 4.16$ Å

Reflection Indices (hkl)	d (Å)	2θ (deg) for CuK_α, $\lambda = 1.5405$ Å
(111)	2.40	37.44
(200)	2.08	43.47
(220)	1.47	63.19
(311)	1.25	76.07
(222)	1.20	79.86
(400)	1.04	95.56
(331)	0.95	108.34
(420)	0.93	111.82

The corresponding interplanar spacings and Bragg reflection angles are not substantially different from those in Table 1. The most recent of these investigators[16] commented that fcc Mo is favored by condensation in poor vacuum conditions onto low temperature substrates. It should also be noted that the fcc modification is usually most pronounced in the first few tens of angstroms of film thickness. Further, high adatom energies, high adatom fluxes, and high substrate temperatures would be expected to produce suppression of fcc structure. Thus, conditions of this investigation would not favor fcc Mo formation unless such formation was strongly promoted by epitaxial or pseudomorphic growth. This observation was confirmed by the absence of fcc Mo peaks in the digitally recorded diffractometer data of this study.

Formation of Substitutional Solid Solutions. The possibility of peak splitting produced by the formation of substitutional solid solutions of Cu in Mo and Mo in Cu was examined. If Cu retained its size of approximately 2.56 Å (from its fcc structure) and Mo retained its size of approximately 2.73 Å (from its bcc structure) and if Cu was substituted for Mo in the Mo lattice, then a reflection corresponding to decreased Mo (110) interplanar spacing would be predicted. In addition, if Mo was substituted in the Cu lattice, a reflection corresponding to increased Cu (111) interplanar spacing would be predicted. These reflections were observed, but an accompanying reflection corresponding to Cu (111) planes with decreased interplanar spacing was also observed. Thus, solid solution strains could account for the peak splitting attributed to Mo (110) planes and one of the peaks attributed to Cu (111) planes. However, the other peak attributed to Cu (111) planes could not be displaced to its observed interplanar spacing by formation of a solid solution.

Accommodation Strains. Accommodation strains resulting from crystallographically related growth of the Cu and Mo layers may have been responsible for the displacement of the Cu (111) peak and, in addition, may have been partly responsible for the other peak positions. Strains implied by the peak locations are indicated in Figure 1. Because Cu has a lower

modulus than Mo, strain would be expected in the Cu lattice to a larger extent than in the Mo lattice, and this may account for the displacement of the Cu (111) peak that was not attributable to solid solution strains. The observed compressive strain of 1.25% in Cu (111) interplanar spacing is high but not unreasonable for this effect.

Annealed Structure

The result of a 2-hr, 750°C heat treatment on the x-ray diffraction pattern is illustrated in Figure 3. Note that there is no evidence of peak splitting in the regions of the Mo (110) and Cu (111) reflections.

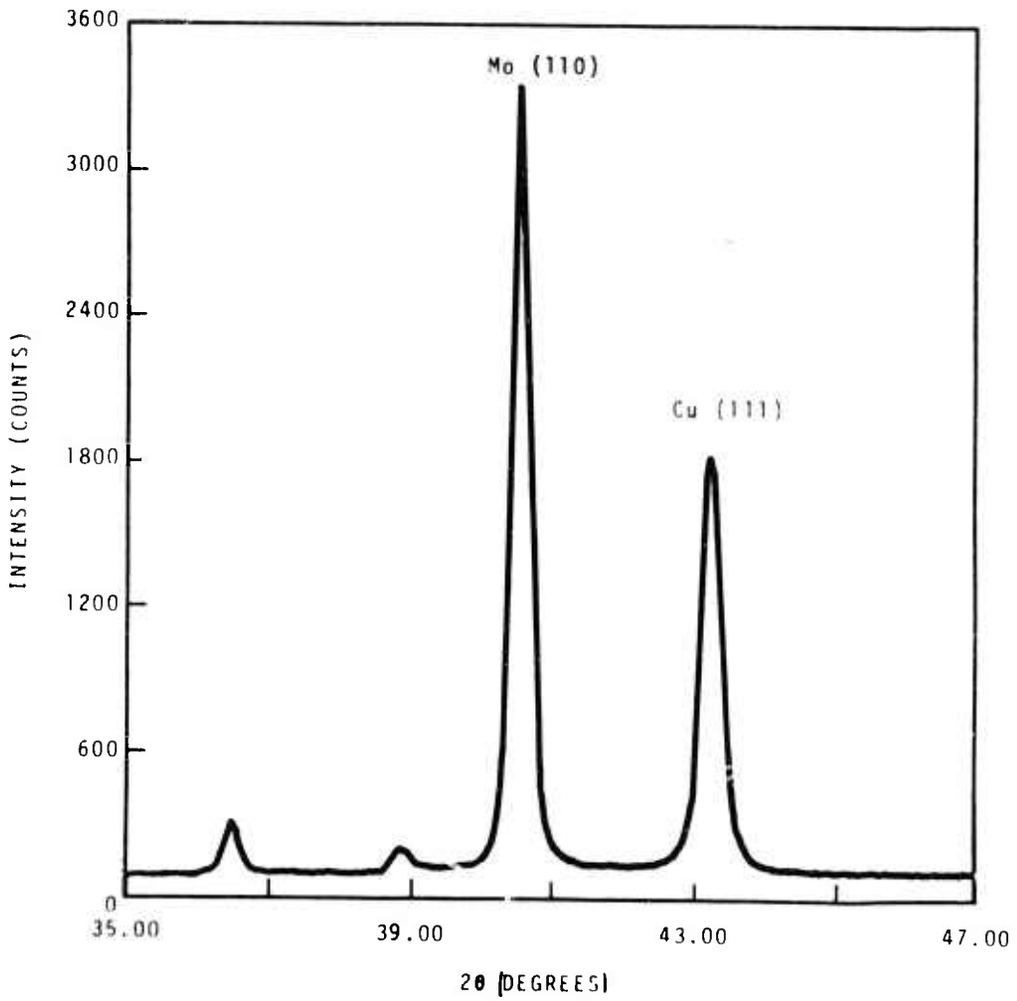

FIGURE 3. Diffractometer Pattern of OTLC-2 After Heat Treatment at 750°C for 2 Hr

Transmission Electron Microscopy

Previous work[6] indicated that for times in the 2- to 4-hr range, breakup of the layered structure by spheroidization occurred between 500 and 750°C. Anneals at 650°C for 1 and 4 hr were evaluated during this reporting period to gain insight as to the nature of the breakup of the layered structure. A summary of the dependence of structure (layered or spheroidized) and sphere diameter on time and temperature is presented in Table 2. The structures of selected heat treated specimens are compared in Figure 4 to the 3-hr, 500°C heat-treated structure which is identical to the as-deposited structure. Note that after 1 hr at 650°C, Figure 4b, the layers were just beginning to break up by spheroidization across several layers with the spheres tending to align in arrays perpendicular to the layer planes. The white Cu phase seemed to be forming a matrix for the dark spheroidizing Mo phase. After 4 hr at 650°C, Figure 4c, layer breakdown had progressed further, and after 2 hr at 750°C it was complete, Figure 4d. Here, the shape and size of Mo spheres, the extent of the Cu matrix, and the absence of Kirkendall-type voids indicates that Mo and Cu must have diffused in a direction perpendicular to the layer planes. Diffusion may also have occurred simultaneously parallel to the layer planes, however, as no evidence to the contrary was observed.

TABLE 2. Influence of Heat Treatment on Microstructure of Deposit OTLC-2

Heat Treatment Temperature (°C)	Time (hrs)	Microstructure	Approximate Mean Layer Thickness or Sphere Diameter (Å)
500	3	Layered	80
650	1	Transition	80
650	4	Transition	80
750	2	Spheroidized	860
1000	2	Spheroidized	2130
1000	4	Spheroidized	3000

a. Heat Treated for 3 hr at 500°C. Microstructure unchanged from as-deposited condition. 100,000X

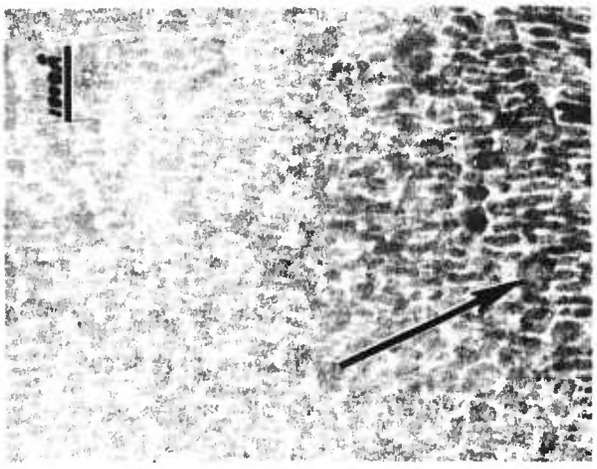

b. Heat Treated for 1 hr at 650°C. Onset of spheroidization. White network phase is Cu, dark phase is Mo. Mo sphere indicated by arrow. 100,000X

c. Heat Treated for 4 hr at 650°C. Additional layer breakdown and spheroidization. 60,000X. Layers perpendicular to arrow.

d. Heat Treated for 2 hr at 750°C. Layered structure completely absent. Mo spheres (dark phase) are ~860 Å in diameter. 51,000X

FIGURE 4. Influence of Heat Treatment on Microstructure of Deposit OTLC-2 as Viewed Parallel to Layer or Prior Layer Planes Which Are Aligned with the Horizontal in the Micrographs

TEM data were not obtained that clearly identify coarsening mechanisms at intermediate temperatures and times, although mechanisms involving both diffusion of Mo through Cu and coalescence of Mo were suspected. As reported previously[6] later stages of Mo sphere coarsening seemed to proceed, at least in part, by coalescence.

Tensile Properties

Since tensile specimens of as-deposited composites produced brittle fractures it was speculated that plastic deformation would not be exhibited in lamellar composite until the Mo sphere size was of the order of 2000 Å. This dimension would be large enough to permit significant dislocation motion. Based on this speculation, samples of TLC-2 were heat treated at 1000°C for 4 hr to cause spheroidization of the microstructure (sphere diameter ~3000 Å), creep-flattened between flat Mo plates during the heat treatment, and then tensile tested at room temperature. As was expected, sufficient ductility was created by spheroidization to allow consistent tensile test results to be obtained. Measured ultimate tensile strengths obtained from three samples averaged 9210 kg/cm^2 (131,000 lb/in.^{2}), or slightly higher than the 8800 kg/cm^2 (125,000 lb/in.^{2}) calculated from hardness data. It was concluded, therefore, that the method used to calculate σ_u from hardness was generally conservative and actual ultimate strengths would be higher than calculated values.

Density

The measured density of as-sputtered composites was 9.51 g/cm^3. Since the average of the densities of Cu and Mo is 9.58 g/cm^3, the lower-than-expected density could be due to a high vacancy concentration or micro-porosity associated with growth defects. It is more likely, however, that slightly more Cu than Mo was sputtered and incorporated in the composite.

Scanning Electron Microscopy

Fracture surfaces of specimens from OTLC-2 were examined in a scanning electron microscope (SEM). Photographs of these surfaces are presented in

Figure 5. The fractures in the as-sputtered material (Figure 5a) and the 550°C heat-treated material (Figure 5b) were typical cleavage fractures. The fracture in the 982°C heat-treated material (Figures 5c and 5d) seems to have followed the Mo sphere-Cu matrix boundaries since the fine cellular structure has a cell diameter of 2 to 3 x 10^{-5} cm (2000 to 3000 Å) which corresponds to the Mo sphere diameter in this material (Table 2).

Resistivity

Resistivity data were obtained as a function of time at a number of temperatures to obtain additional insight as to the nature of the lamellar composite and its response to heat treatment. In addition, the resistivity data permitted calculation of activation energies for the thermally activated processes responsible for structural changes and thus provided insight as to possible mechanisms for the changes. Tabulations representative of the resistivity data obtained and its treatment are presented in Appendix I. Table 3 and Figure 6 summarize the influence of time on corrected resistivity at selected temperatures. In general, within the first minute of exposure to the hot fluidized bed, Figure 6, resistivity increased to a peak value as the test temperature is reached by the sample and then decreased very rapidly. As time increased for temperatures in excess of 750°C, resistivity decreased to a nearly equilibrium value characteristic of the "fully annealed" condition. For lower temperatures, of course, intermediate resistivity values characteristic of the particular partially annealed condition were obtained.

Residual Resistivity of As-Deposited Condition

Since the ~4 μΩ cm resistivity characteristic of the nearly equilibrium condition is at least a factor of three lower than that in the as-deposited condition, Table 3, it is pertinent to consider possible sources of the added resistivity in as-deposited material. Matthiessen[17] discovered that the resistance of a metal is equal to the sum of the temperature-dependent resistance [$\rho(T)$] of the pure metal's undisturbed lattice and the residual resistance (ρ_0) due to effects which limit the electron mean-free path.

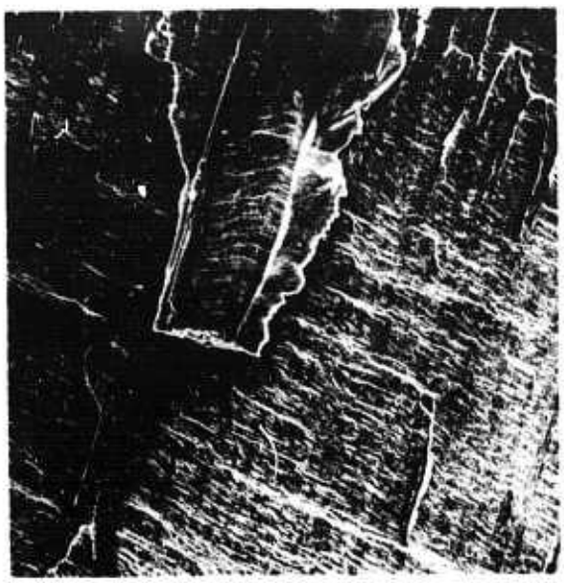

a. As-Deposited. 600X

b. Heat Treated at 550°C for 17 hr. 850X

c. Heat Treated at 982°C for 55 min. 500X

d. Heat Treated at 982°C for 55 min. 5000X

FIGURE 5. SEM Fractographs of Composite OTLC-2 in Various Conditions

TABLE 3. Influence of Temperature on Resistivity of Lamellar Composite

Specimen Number	As-Deposited ρ (μΩ cm)	As-Deposited Temp.(a) (°C)	After Thermal Cycle to Indicated Temperature: Temp. (°C)	ρ at 25°C (μΩ cm)	ρ at -196°C (μΩ cm)
OTLC-2	14.18	38	982	3.57	0.95
OTLC-2	13.85	31	837	3.63	1.10
OTLC-2	11.73	31	754	3.88	1.56
OTLC-2	15.10	36	641	5.45	2.68
OTLC-2	14.70	26	622	5.20	--
OTLC-2	14.58	28	550	9.82	6.93
TLC-2	22.10	32	976	4.76	1.26
TLC-2	14.53	26.2	311	4.20	1.26

a. Temperature of measurement.

This may be expressed as Matthiessen's rule, $\rho = \rho_0 + \rho(T)$. In the present work, then $\rho(T) = \sim 4$ μΩ cm and ρ_0 equals the difference between $\rho(T)$ and the as-deposited value or ~10 μΩ cm.

Since the starting materials were quite pure for these experiments and since the equilibrium insolubility of Mo and Cu[18] indicated that very little Cu-Mo solid solubility was expected, the residual resistivity may have resulted from a combination of elastic strain, quenched-in lattice defects during sputter deposition, and small grain size and/or thin layer (thin film) effects as discussed below.

Elastic Strain. Within the elastic limit, deformation of metals is not expected to result in large changes in resistivity.[19] Large resistivity changes due to pressure have been observed, however, up to as large as a factor of 4 increase[20] for pressures near 2×10^4 kg/cm^2. This is approximately 1% of the observed modulus of the Cu-Mo composite and thus corresponds to about 1% elastic deformation. Since x-ray diffraction

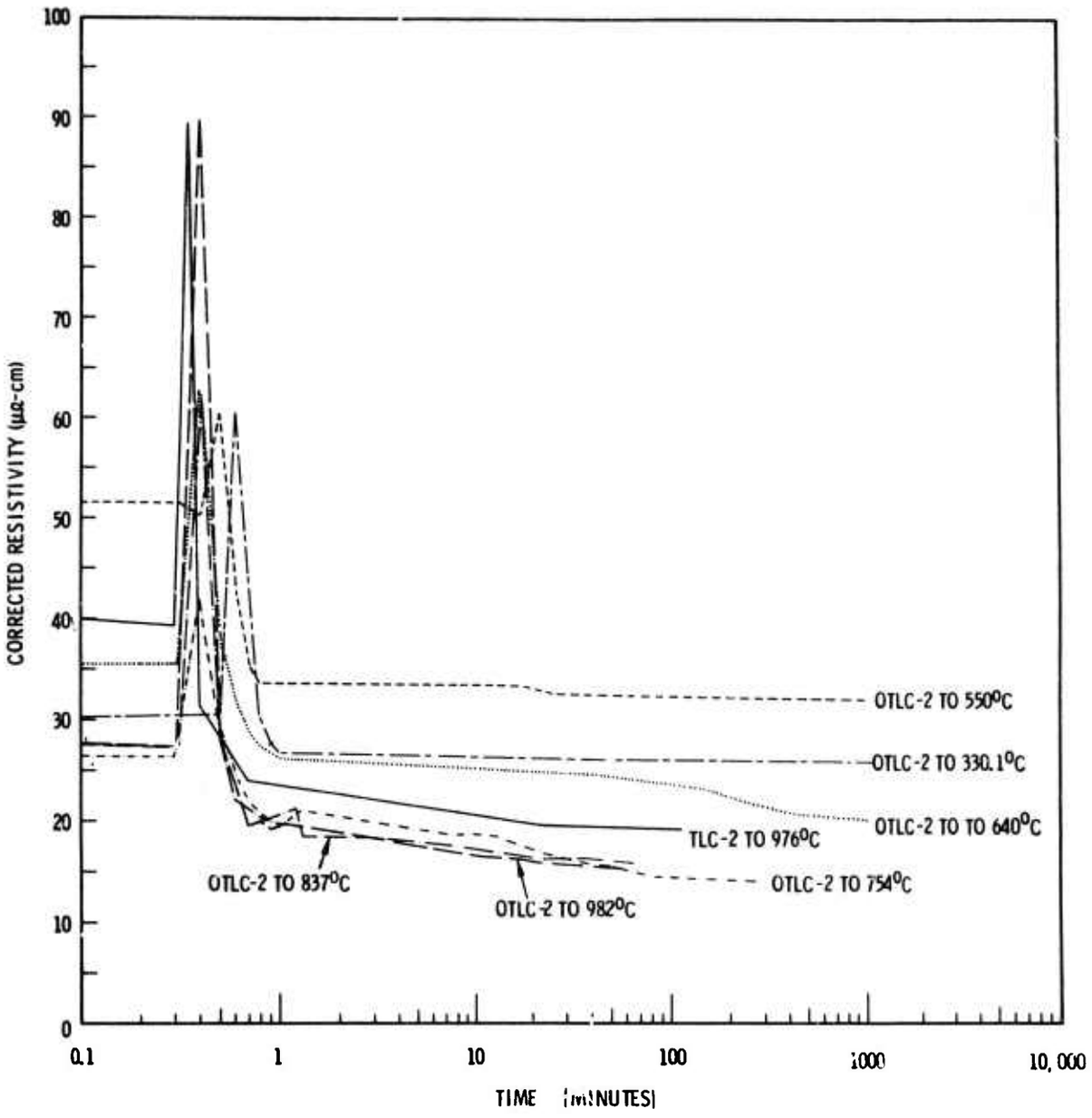

FIGURE 6. Time Dependence of Resistivity, Corrected to 982°C from Isothermal Resistivity Measurements at Several Temperatures

evidence for lattice distortion approaching this value has been identified in a previous section it is possible that elastic distortion may be responsible for a large part of the residual resistivity.

Quenched-In Vacancies. Since the adatom surface temperature during sputter deposition has been calculated to be of the order of 30,000°K[9,21] the possibility of quenching-in vacancies during deposition is very strong. If vacancies are retained in the proportion exp (-Q/kT), where Q is the activation energy for vacancy formation and T is the surface temperature, then a surface temperature of only 3000°K is adequate to obtain 1 at.% vacancies. Since the calculated resistivity associated with 1 at.% of vacancies, including resistivity resulting from vacancy strain fields, is 1.5 μΩ cm,[22] it is possible that quenched-in vacancies could contribute to residual resistivity.

Grain Size and/or Thin-Film Effects. Small grain size and thin film effects may be treated collectively if the composite is considered as an aggregate of thin films with grain size related to film thickness. The Fuchs[23] theory as modified recently by Mayadas and Shatzkes[24] and Mola and Heras[25] (including grain size effects) predicts a resistivity increase over bulk Cu values by a factor of approximately 3 for films 50 to 100 Å thick. An excellent early correlation with theory for thin film thicknesses in this range was given by Reynolds and Stilwell.[26] Approximately 10 to 15 μΩ-cm of the as-deposited resistivity, then, could be accounted for by thin-film effects.

Conclusion. In conclusion, then, approximately 10 to 15 μΩ-cm can be accounted for by thin film effects with a refined Fuchs theory. Any remaining residual resistivity can be accounted for by elastic strain effects and effects due to quenched-in defects. These effects must be very strong, however (also evidenced by x-ray diffraction and hardness data) since cold work only results in resistivity increases of approximately 18% in Mo[19] and 1.6% in Cu.[27] Other contributions to the resistivity may also be active, but the observed room-temperature resistivity values are in the range of values to be expected from such structures.

Analysis of Resistivity Data

The large effect on resistivity expected from the thermally activated modifications of the thin-layered structure indicated that resistivity changes should be a good measure of structure changes during breakdown of the layered structure and early coarsening of the resulting spheroidized structure. Resistivity was not expected to be a good measure of the later stages of sphere coarsening because at 750 to 1000°C the Mo sphere size very soon exceeds the electron mean free path. Therefore further resistivity change would be expected to be small.

Considering the thermally activated processes causing changes in resistivity, an Arrhenius analysis was used to obtain activation energies for mechanistic speculations. Here reaction rate (R) was assumed to be proportional to the time rate of change of resistivity and related to temperature according to $R = \Delta\rho/\Delta t = \text{const. } \exp(-Q/kT)$, where ρ is the measured resistivity, t is time, Q is the activation energy, and T is the temperature at which resistivity measurements were carried out. Temperature corrections to the resistivity data and the procedures used to determine activation energies from the corrected resistivity data are described in Appendices I and II, respectively.

The results of the activation energy determinations are summarized in Table 4. Based upon these data and a review of relevant published activation energy data detailed in Appendix III, the following observations were made. The early structural changes prior to layer breakdown produced by heat-treatment were characterized by an activation energy of 9.63 kcal/mole, a value appropriate for vacancy migration to sinks. The next stage of structural change, indicated by activation energies of 10.18 to 22.06 kcal/mole (resistivities from 22 to 35 μΩ-cm), may have been closely related to the first stage and was probably produced by grain boundary or interface diffusion of Cu and Mo. This second stage structural change produced layer breakdown by Mo spheroidization. The third and final stage observed was characterized by an activation energy of 69.85 kcal/mole (resistivity from 20 to 25 μΩ-cm) and produced Mo sphere coarsening. Mo sphere coalescence produced by Mo diffusion through the Cu matrix or other means was identified

TABLE 4. Activation Energy Associated with Structural Change as Indicated by Resistivity

Structure as Characterized by Resistivity, $\rho_{982°C}$ ($\mu\Omega$-cm)	Activation Energy (kcal/mole)
40	9.63
35	17.00
33	18.90
30	22.06
28	14.21
25	53.27 (11.33[a])
24	52.88 (10.18[a])
22	58,80 (11.33[a])
20	69.85
17	0
16	0

a. See Appendix II for a discussion of these values.

as a possible source of this third stage phenomenon. Note that two structural change processes may be occurring simultaneously in the structure characterized by resistivities of 22 to 25 $\mu\Omega$-cm.

Analysis of Hardness Data

If an Arrhenius[28] analysis is applied to the hardness data presented previously[6] using the rate of change of hardness as a measure of structural change and assuming a thermally activated process, then the rate is given by

$$\text{Rate} = \text{const. exp } (-Q/kT)$$

and the results in Table 5 are obtained. Here Rate (average) = $\Delta(\text{DPH})/\Delta t$, $\Delta(\text{DPH})$ = hardness change, Δt = time at temperature, T = heat treatment temperature, and Q = activation energy.

TABLE 5. Calculation of Arrhenius Parameters from Hardness Measured at Room Temperature After Heat Treatment

Sample	1/T ($°K^{-1}$ x 10^{-3})	Δ [DPH]	Δt (Hr)	Rate	ln [Rate]
TLC-4, As sputtered surface					
H.T. @ 750°C 0-1 hr	0.977	0	1	--	--
1-2 hr	0.977	36	1	36	--
H.T. @ 1000°C 0-2 hr	0.786	253	2	126.5	4.840
OTLC-2, polished surface					
H.T. @ 750°C 0-2 hr	0.977	184	2	92	4.522
H.T. @ 1000°C 0-1 hr	0.786	326	1	326	5.787
TLC-4, polished surface					
H.T. @ 500°C 0-1 hr	1.294	57	1	57	4.043
H.T. @ 636°C 0-1 hr	1.100	115	1	115	4.745
H.T. @ 788°C 0-1 hr	0.943	261	1	261	5.565
H.T. @ 987°C 0-1 hr	0.794	344	1	344	5.841

The Arrhenius plots of ln (Rate) versus 1/T are shown in Figure 7. Activation energies Q obtained from this plot ranged from 14.9 kcal/mole to 26.4 kcal/mole. Because of the very small amount of data and its nature, however, these activation energies are given with reservation and are approximate at best. They correspond to average rates and compare very well with the 14.21 to 22.06 kcal/mole range of values obtained from resistivity data for the second stage of the annealing process.

COMPOUND-FORMING SYSTEMS

The results of the first phase of this program[6] indicated the following:

a. The strengthening effect of the lamellar structure, as measured by the flow stress at a selected value of strain, depended in the expected manner on the volume (thickness) fraction of the reinforcing (compound) layers and the thickness of the layer pair repeating units.

b. However, the fracture stress of the lamellar composites exhibited the opposite dependence on the above parameters, being determined

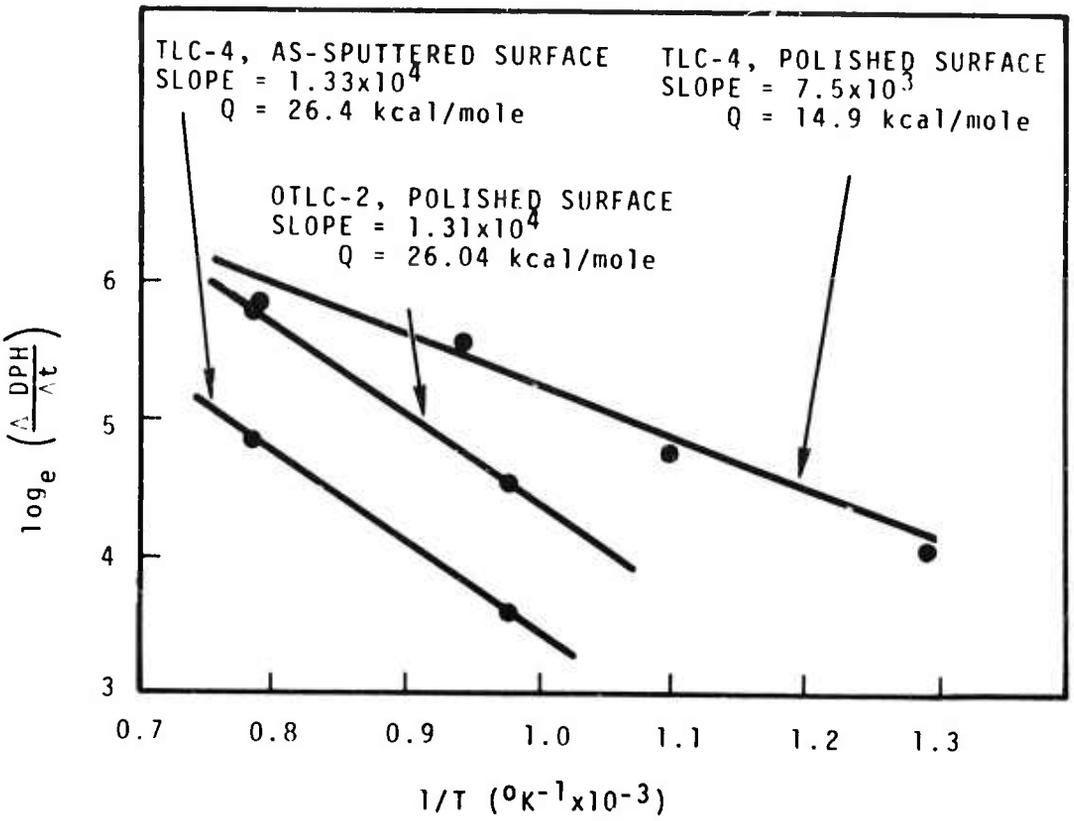

FIGURE 7. Arrhenius Determination of Activation Energy from Hardness Changes with Heat-Treatment Temperature

by the strain to fracture. This property was an order of magnitude greater in the case of the smaller fraction of reinforcing layers.

The direction of the second phase of the program was based on the above results. Specimens of the Ti-BeTi composite system were prepared with smaller fractions of the reinforcing Be-Ti layers. The thickness of the Ti layers was increased in an attempt to increase plasticity by reducing the constraints imposed by the reinforcing layers. These specimens exhibited significantly higher fracture strengths.

Although this result was in the desired direction it was not considered sufficient to establish the engineering feasibility of this class of material. Therefore, alternate composite systems were selected, based on aluminum as

the "matrix," or element to be reinforced. The intermetallic compounds, $NiAl_3$ and $TiAl_3$, and elemental beryllium, were investigated as reinforcing agents.

MATERIALS AND PROCEDURES

Sputtering targets were fabricated from commercial purity metals. Aluminum and beryllium were obtained as 6-in. diameter bar; titanium and nickel were obtained in 1/4-in. plate. The semicylindrical targets were paired, as shown in Figure 8, to form the lamellar composites. The exposed area of the strips inserted in the segmented half target was selected on the basis of yield data published by Wehner[29] and the composition of the desired intermetallic compounds. The targets were independently biased to control the relative deposition rates of the metal and compound, and thus the thickness of the respective layers. The substrate was a cylinder concentric with the targets and rotated at a rate selected to obtain a desired layer pair thickness in the deposit. The deposition and sample preparation procedures have been previously reported.[6] The depositions performed during the reporting period are listed in Table 6.

RESULTS AND DISCUSSION

Ti-BeTi Composites

Two additional titanium-beryllium deposits were produced during this phase of the program. The first (Deposit 15), employed the segmented target scheme previously described,[6] with altered rotation speed and voltage ratio to produce thicker titanium layers and thinner compound layers (i.e., smaller amount of reinforcement). The second deposit (16) was made with pure elemental targets (Ti and Be) so that formation of the compound would be purely by interdiffusion. Both experiments were intended to increase plasticity, since the strength of previous deposits was restricted by inadequate plasticity. The deposition data are presented in Table 6.

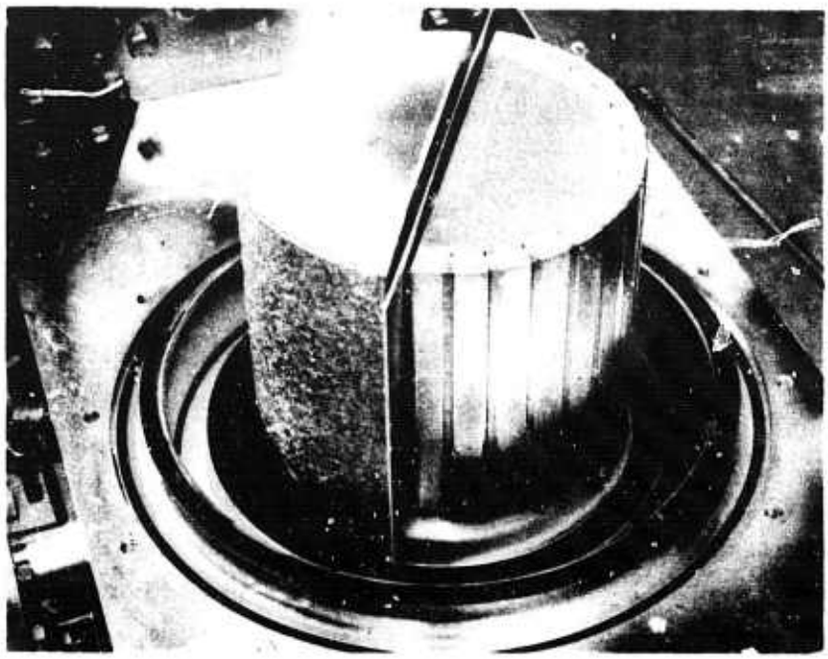

FIGURE 8. Sputtering Target Used to Deposit Lamellar Composites of Al-NiAl. The semicylinders are pure aluminum; one is plain and the other has nickel insets to produce the NiAl layer.

TABLE 6. Deposition Parameters for Ti-BeTi Composites[a]

Target Pair	Run No.	Voltage Ratio	Substrate Rotation (rpm)	Substrate Temp. (°C)	Deposition Rate (mil/hr)	Deposit Thickness (mils)
Ti-BeTi	15	0.25	0.3	500	0.4	0.014
Ti-Be	16	0.25	0.3	500	0.4	0.011
Al-AlNi	17	0.17	0.3	300	0.9	0.008
	18	0.17	0.3	300	0.9	0.018
	19	0.13	0.7	250	0.8	0.020
	24	0.20	0.7	70	0.8	0.018
Al-AlTi	20	0.20	0.3	250	0.8	0.019
	21	0.35	0.3	250	0.9	0.021
	22	0.20	0.7	250	0.8	0.018
Al-Be	23	0.35	0.3	250	0.7	0.017
	25	0.46	1.0	70	0.8	0.019

a. Substrate potential was floating (-20 V) in all depositions.

Mechanical Properties

Room temperature tensile and three-point bend tests were conducted on these materials in both the as-deposited and the heat-treated (1 hr at 700°C) conditions. The results are shown in Table 7.

TABLE 7. Properties of Ti-BeTi Lamellar Composites in Tension and Bending

			Bend Testing	
Deposit	Condition	Tensile Strength, (ksi)	Maximum Fiber Stress, (ksi)	Plastic Strain
15	AD[a]	88.75	437.8	~0
	HT[b]	--	392.9	~0
16	AD[a]	104.15	499.1	8×10^{-3}
	HT[b]	--	465.9	2×10^{-3}

a. AD = As-Deposited.
b. HT = 1 hr at 700°C.

The plastic strain exhibited in the tensile tests was on the order of 10^{-5}, i.e , the specimens were very nearly elastic. In part, this behavior was due to gripping difficulties. In the three-point bend tests, Deposit 15 behaved in an elastic manner, but Deposit 16 exhibited an obvious curvature in the load-deflection plot.

Although it is not strictly valid to correlate stresses and strains in three-point bending with tensile properties, such a correlation was made as a first approximation for Deposit 16. The plastic deflections corresponded to plastic strain of 8×10^{-3} in the as-deposited specimen, and 2×10^{-3} in the heat-treated specimen. The "yield strengths" at 2×10^{-3} (0.2%) were 456 and 466 ksi, respectively.

The data confirms the previously observed dependence of the achieved strength on the plasticity, or ability to deform, of the deposits. This dependence arises from the extremely high work-hardening rates of these materials (approximately E/2) in the microstrain region.

Microstructure

The microstructure of these materials was evaluated from the fracture surfaces of bend-test specimens by scanning electron microscopy, Figure 9. The lamellar structure of Deposit 15 was not visible on the unetched fracture surface, which had a glassy appearance. In the etched structure, Figure 9a, the apparent thickness of the layers versus the gaps between layers indicates that the metallic titanium was selectively dissolved during etching. In Deposit 16, the as-deposited compound layers, formed by interdiffusion between the alternating beryllium and titanium layers, are indicated by the thin irregular white lines, Figure 9b. An attempt was made to further develop this structure by heat treatment at 700°C. No thickening of the compound layers was observed, but the layers became less linear, Figure 9c. The apparent coarsening of the overall layer structure is believed due to an unintentional deviation from a surface perpendicular to the plane of the layers. The difference between the structures of these deposits is attributed to the fact that in one case (15) the compound layers were deposited directly, while in the other (16) they were formed by interdiffusion of the metal layers. Attempts to verify the presence of the intended $TiBe_{12}$ compound by x-ray diffraction were inconclusive. Diffraction peaks attributable to $TiBe_{12}$ and $TiBe_{(10 + n)}$ were observed, but satisfactory patterns (i.e., all expected intense peaks) were not obtained.

Al-NiAl, Al-TiAl and Al-Be Composites

The restricted plasticity of the materials, even in the most favorable condition, discouraged further investigation. Although very impressive strengths were obtained, the applicability to structures was considered small. Therefore, in order to fulfill the program objective of demonstrating the engineering utility of sputtered lamellar composites, it was decided to investigate a series of alternate material systems. Aluminum was selected as the "matrix," or element to be reinforced for these systems primarily for its low density and high plasticity. Aluminum forms strong intermetallic compounds with titanium and nickel; the most aluminum-rich of the compounds in each system was selected as the reinforcing material. This

choice was made primarily on the basis of thermodynamic stability of the composite, and secondarily, minimum density considerations.

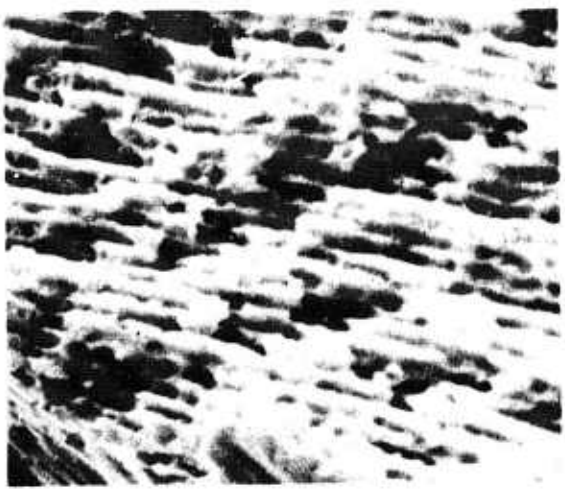

a. Deposit 15, Etched, 8000X

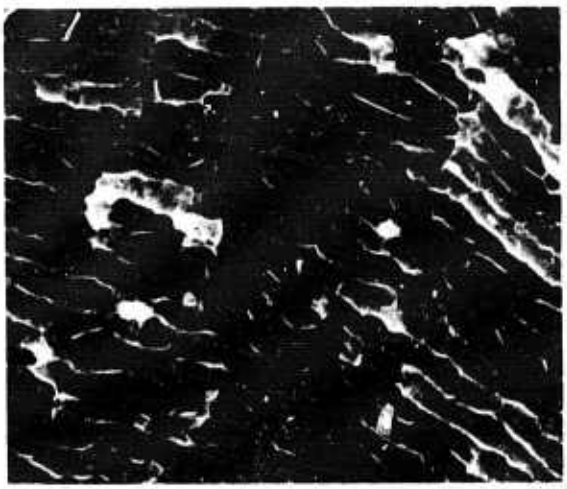

b. Deposit 16, 4000X

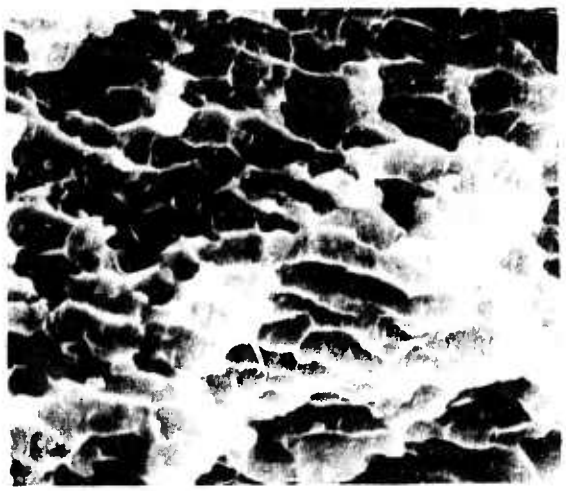

c. Deposit 16, Heat Treated 1 hr at 700°C, 4000X

FIGURE 9. Microstructure of Ti-BeTi Lamellar Composites, Obtained from Fracture Surfaces by SEM

An additional system, using beryllium as the reinforcing element, was also investigated. Although this system was outside the scope of this part of the program, not being a compound-forming system, it was considered attractive since the elastic modulus of beryllium is of similar magnitude to the intermetallic compounds above, and its density is significantly less. Also, no stoichiometry problems exist, which considerably simplifies interpretation of the results.

Deposits of each of these systems were formed with various layer thicknesses, Table 8. In most cases, the substrate temperature was 250°C; two deposits were formed at a low temperature (70°C) to determine whether or not temperature was a significant parameter. The layer thicknesses and corresponding fraction of reinforcing layer are presented as calculated (from total deposit thickness, time and rotation rate), and observed (scanning electron microscope) values.

TABLE 8. Layer Thickness Data

		Calculated Thickness (μm)			Observed Thickness (μm)		
Number	Identity	Aluminum	Reinforcement	%(a)	Aluminum	Reinforcement	%(a)
17	Al-Ni	0.92	0.23	20	1.04	0.34	25
18		0.96	0.14	13	0.88	0.19	18
19		0.45	0.08	15	0.47	0.11	19
24(b)		0.39	0.13	25	0.34	0.16	32
20	Al-Ti	0.88	0.12	12	0.78	0.22	22
21		0.82	0.29	26	0.82	0.30	27
22		0.41	0.08	16	0.43	0.11	20
23	Be	0.82	0.09	10	0.70	0.12	14
25(b)		0.28	0.05	15	0.25	0.06	19

a. Percent reinforcement.
b. Deposited at 70°C, all others at 250°C.

The discrepancy between calculated and observed thickness values was attributed to the point-to-point thickness variation in the deposits and deviation from perpendicularity of the examined sections to the lamellar structure. In all cases, the observed reinforcement is larger than calculated, perhaps due to overestimation of the thickness of the thinner layers.

The calculated values are considered more accurate, and will be used as the basis for comparison of mechanical property results.

Mechanical Properties

The mechanical properties of the deposits were determined by room temperature tensile and three-point bend tests, and tensile tests at 300 and 400°C. The results are shown in Tables 9, 10 and 11 and Figures 10 and 11.

The only comparison which can be made with the literature is for the case of Al-NiAl. This system has been produced in lamellar form by directional solidification at compositions of 6 to 11 wt% nickel. Elastic moduli of 11.3 to 11.6 x 10^6 psi and ultimate tensile strengths of 43 to 48 x 10^3 psi were observed.[30,31,32] Comparative values from the present work were appreciably higher due to the greater volume fraction of the reinforcing phase.

The following observations can be made from the tabulated data:

1. With the exception of Specimen 19, the tensile modulus and elastic limit correlate with the corresponding properties in three-point bending. The tensile moduli were ∿25% greater than those observed in bending, while the bend strengths were about three times those observed in tension. The lower moduli in bending are traceable to the use of crosshead motion for strain measurement, in place of strain gauges as used for tensile tests. The greater strengths in bending are partly due to the effects of longitudinal curvature of the tensile samples and partly due to the fact that only a small volume is subjected to maximum tension in the bend test; thus decreasing the probability of encountering a critical flaw.

2. With the exception of microhardness, where the expected dependence was observed, the mechanical properties of the composites reinforced by AlNi and AlTi were not consistently dependent on the layer thicknesses or the percent reinforcement. Such a dependence was expected theoretically[33] and has been generally observed in other work[30,34] and previous work in this program.[6] The

TABLE 9. Room Temperature Tensile Properties

Number	Identity	Elastic Modulus (10^6 psi)	Stress at Indicated Plastic Strain (10^3 psi)				Total Strain, (%)	Hardness, (DPH)
			<10^{-4}	2×10^{-4}	2×10^{-3}	Fracture		
17	Al-Ni	12.95	26.23	--	--	--	0.2	121
18	Al-Ni	15.34	24.17	27.37	48.65	54.72 (3×10^{-3})	0.6	93
18	Al-Ni(a)	14.66	17.90	20.77	44.32	49.19 (3×10^{-3})	0.6	--
19	Al-Ni	11.71	22.96	27.84	41.87	--	0.5	92
24	Al-Ni(b)	13.66	39.56	52.32	--	57.30 (4×10^{-4})	0.3	224
20	Al-Ti	12.26	22.08	25.54	64.58	--	0.7	120
21	Al-Ti	12.49	18.62	22.21	54.02	--	0.6	124
22	Al-Ti	11.83	21.29	24.13	46.13	59.61 (4×10^{-3})	0.9	122
23	Be	13.01	26.14	29.26	--	43.30 (8×10^{-4})	0.4	104
25	Be(a)	14.14	50.16	--	--	--	0.3	167

a. Heat treated 1 hr at 400°C.
b. Low substrate temperature.

TABLE 10. Room Temperature Bend Tests

Number	Identity	Stress at Indicated Strain (10^3 psi) <10^{-4}	Stress at Indicated Strain (10^3 psi) Fracture	Elastic Modulus (10^6 psi)
17	Al-Ni	124.7	124.7 (<1 x 10^{-4})	9.89
18	Al-Ni	81.5	161.6 (4 x 10^{-4})	10.15
19	Al-Ni	118.9	118.9 (<1 x 10^{-4})	10.54
24	Al-Ni	149.1	149.1 (<1 x 10^{-4})	11.50
24	Al-Ni[a]	137.7	137.7 (<1 x 10^{-4})	10.50
20	Al-Ti	104.5	219.2 (19 x 10^{-4})	9.51
21	Al-Ti	66.7	255.5 (8 x 10^{-4})	9.50
22	Al-Ti	60.9	281.6 (16 x 10^{-4})	9.01
22	Al-Ti[a]	174.5	240.2 (7 x 10^{-4})	10.02
23	Be	59.9	145.1 (5 x 10^{-4})	11.10
25	Be	194.1	194.1 (<1 x 10^{-4})	12.55
25	Be[a]	151.2	151.2 (<1 x 10^{-4})	11.66

a. Heat treated 1 hr at 400°C.

TABLE 11. Elevated Temperature Tensile Properties

Deposit Number	Identity	0.2%[a] Yield Strength, (ksi)	Ultimate Tensile Strength, (ksi)	Elongation (Percent)
		Tested at 300°C (0.61 Tm)		
19	Al-Ni	7.61	11.92	6.7[b]
24	Al-Ni	11.43	13.21	4.2[b]
21	Al-Ti	23.09	35.57	1.8
23	Be	20.38	27.69	2.7
25	Be	25.37	34.81	2.8
		Tested at 400°C (0.72 Tm)		
21	Al-Ti	6.59	10.35	9.0
25	Be	12.46	12.46	8.5

a. Approximate offset from crosshead motion.
b. Reduction of area >80%.

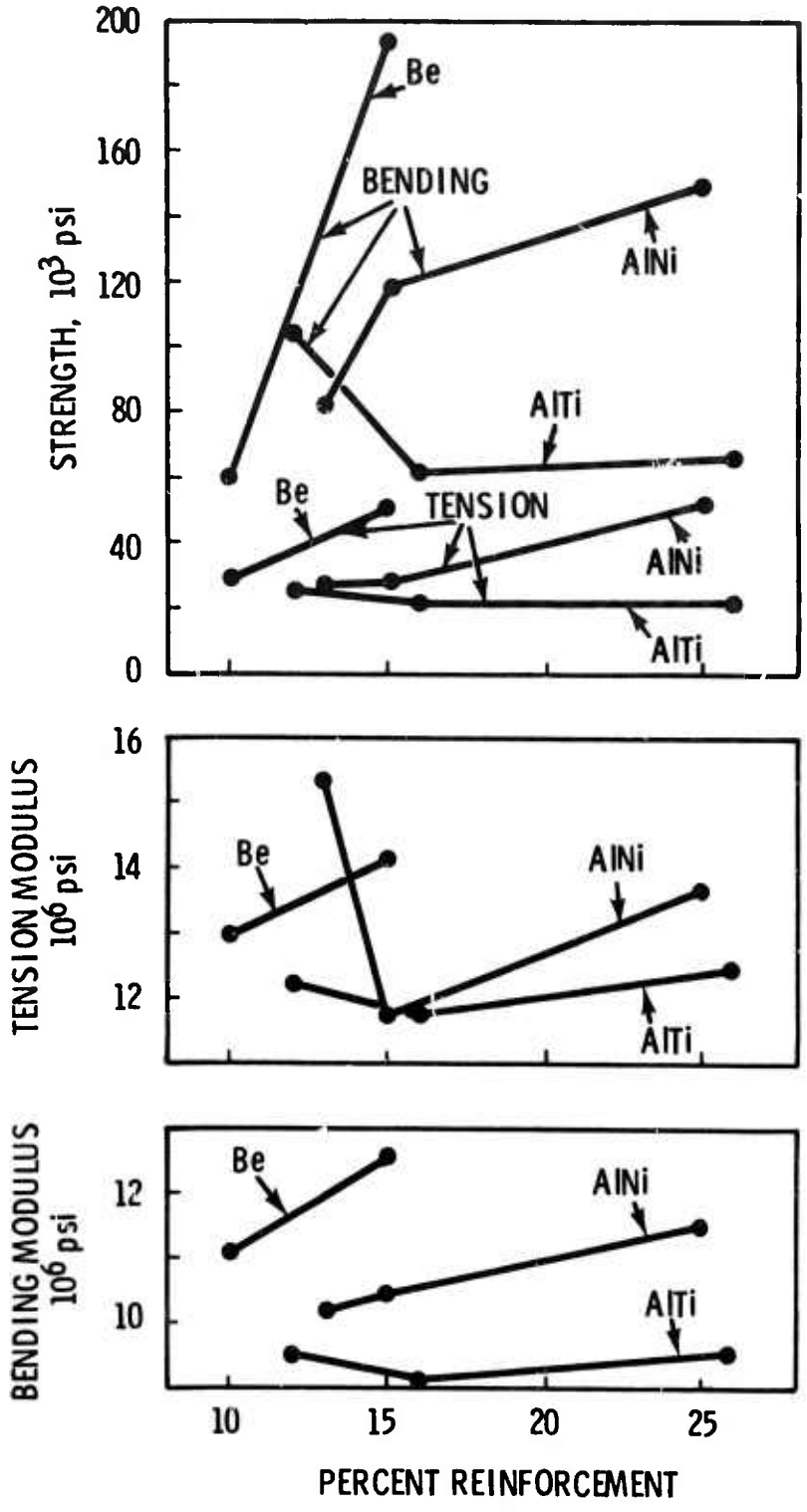

FIGURE 10. Room Temperature Mechanical Properties of Lamellar Composites Versus Percent Reinforcement

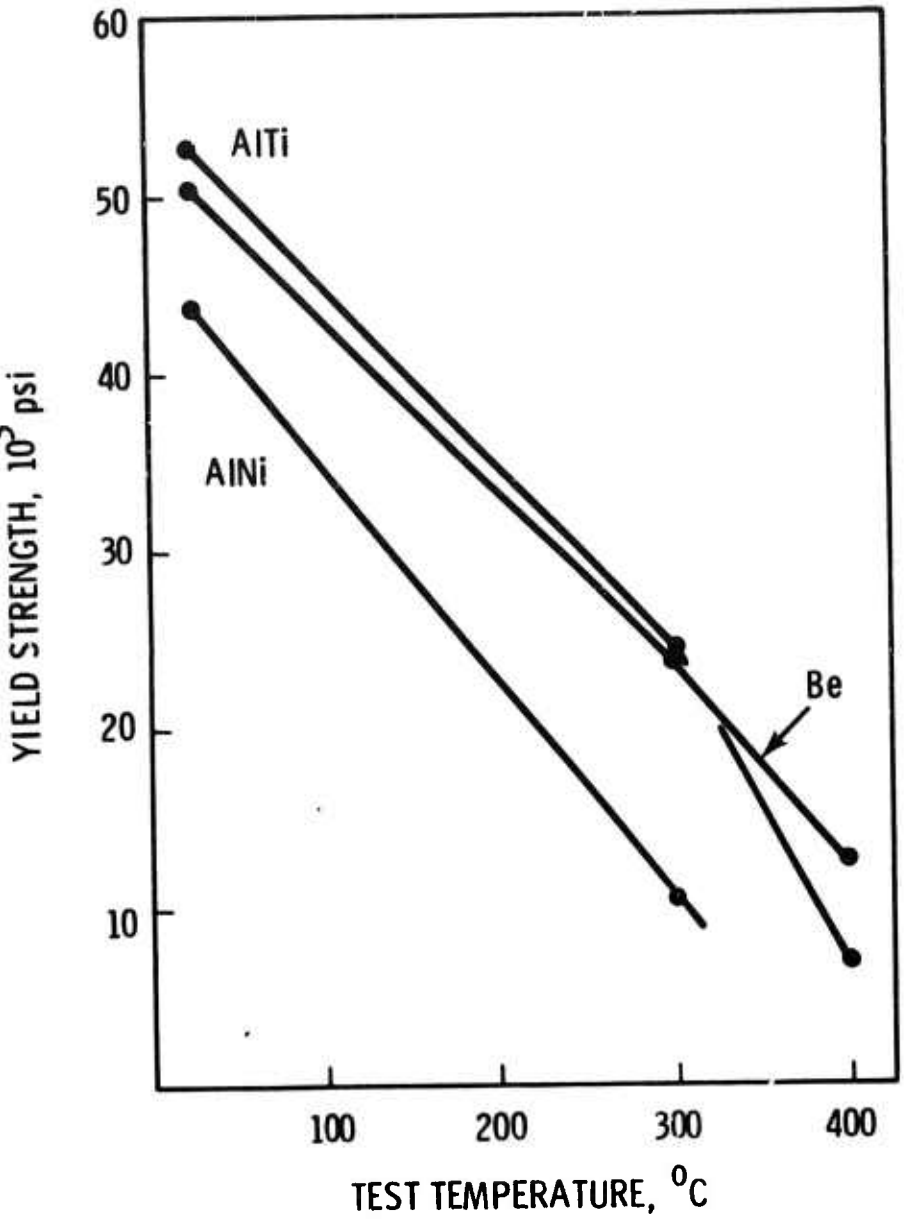

FIGURE 11. Temperature Dependence of the Yield Strength of Lamellar Composites

absence of the expected dependence in the bend and tensile data may be due to one or more of the following:

a. Cracking of the reinforcing layers would reduce their effect on the elastic modulus and strength of the composites. If the extent of cracking was proportional to the fraction of the reinforcing layers (i.e., volume %), the expected dependence of mechanical properties could be effectively canceled. Such cracking was not observed metallographically, and was apparently not extensive (if present at all) since the composites did exhibit elastic moduli 30 to 60% greater than aluminum.

b. Incomplete formation of the intermetallic compound would be expected to affect mechanical properties similarly to cracking of the compound layers. This effect was present in the Al-Ti system, which showed a substantial increase in properties after a 400°C heat treatment. Calorimetry of these samples revealed an exothermic reaction attributable to formation of the intermetallic compound. The Al-Ni specimens showed no such reaction and their mechanical properties decreased after heat treatment. This effect, therefore, cannot account for the results in general.

c. Residual stresses in the composites would be expected to affect the observed strengths, and could also influence the elastic moduli. The presence of residual stress was indicated in all composite specimens by changes in shape upon removal from the sputtering apparatus. Al-Ni composites were under tensile stress, while the other systems were under compressive stress. These stresses were relaxed when the substrate was removed. A second stress system, which was not relaxed, arose from the mixmatch in thermal expansivity between the reinforcing layers and the aluminum layers. This mismatch would put the aluminum layers in tension and the reinforcing layers in compression. The measured modulus would be decreased if the aluminum layers were stressed beyond their yield strength.

Since this is more likely with higher amounts of reinforcement, this mechanism may partially or completely cancel the expected increase in modulus with increased reinforcement. Such effects have not been reported in the literature to the authors' knowledge. Residual stresses have been reported to produce a tension-compression strength difference[35] but in that work the elastic modulus was not affected.

3. The Al-$TiAl_3$ composite system exhibited the highest yield strengths in tension. Although the elastic limits were less than selected samples of the other systems, the latter failed at smaller strains and thus did not reach equivalent strength levels. Similar results were obtained in bend testing.

4. The effect of heat treatment at 400°C differed in the various systems. The Al-Be and Al-$NiAl_3$ systems exhibited a loss of strength without an increase in plasticity. In contrast, the Al-$TiAl_3$ system exhibited a large increase in elastic limit, and a reduction of plasticity. This latter result, together with the presence of an exothermic reaction detected by scanning calorimetry, implies that the intermetallic compound forming reaction was not completed during deposition of this alloy system. The measured heat of transformation, 17 kcal/mole, based on the calculated volume fraction of $TiAl_3$, is of the order of the heat of formation of similar compounds. An attempt was made to confirm this by x-ray diffraction, but the results were not conclusive.

5. The yield strength decreased more rapidly with temperature in the Al-$NiAl_3$ samples than in the other systems, Figure 11. Both Al-$TiAl_3$ and Al-Be had strengths over 20 ksi at 300°C, which is 0.61 of the absolute melting point; and Al-Be had a strength of 10 ksi at 400°C, or 0.72 Tm. These samples exhibited small reductions in area, while the Al-$NiAl_3$ system exhibited chisel-point necking with reduction in area >80%.

The decrease in strength with temperature was greater than expected for specimens with stable microstructures. Such composites generally show only a small dependence of strength on temperature. For example, the Ni-Ni_3Nb eutectic system, directionally solidified to form a lamellar composite, exhibits a high fraction of its low temperature strength at 700°C.[36,37] In the present work, it is probable that annealing of the defect structure quenched in by sputter-deposition is responsible for the decrease in strength. Dispersion hardening of the individual layers could be accomplished by co-deposition of small amounts of insoluble materials, and should significantly improve the high temperature strength.

The Al-$NiAl_3$ specimens were unstable when strained at 300 and 400°C. The breakup of the continuous layer structure is shown in Figure 12 where it is seen that the effect is related to the reduction in area as the necked region is traversed. This alloy system has been observed to behave similarly in directionally solidified eutectic form.[30,32] The instability of the continuous layer structure accounts for the more rapid decrease of strength with increasing temperature.

Microstructure

The lamellar structure of the composites was examined by scanning electron microscopy of room temperature fracture surfaces. The Al-$NiAl_3$ composites are shown in Figure 13. Ductile behavior is readily visible in Deposit 17, where the aluminum layers have necked in a chisel-point manner, and to a lesser extent in Deposit 18. The other samples appear to have fractured in a brittle manner. The fracture appearance correlates well with the observed elongations in the tensile tests, Table 9. It should be noted that in no case is any delamination of the layers visible. The non-planar nature of the fracture surface of Deposit 24 may be an indication of the significance of the columnar structure (vertical in the photograph) with respect to fracture in composites deposited at low substrate temperatures.

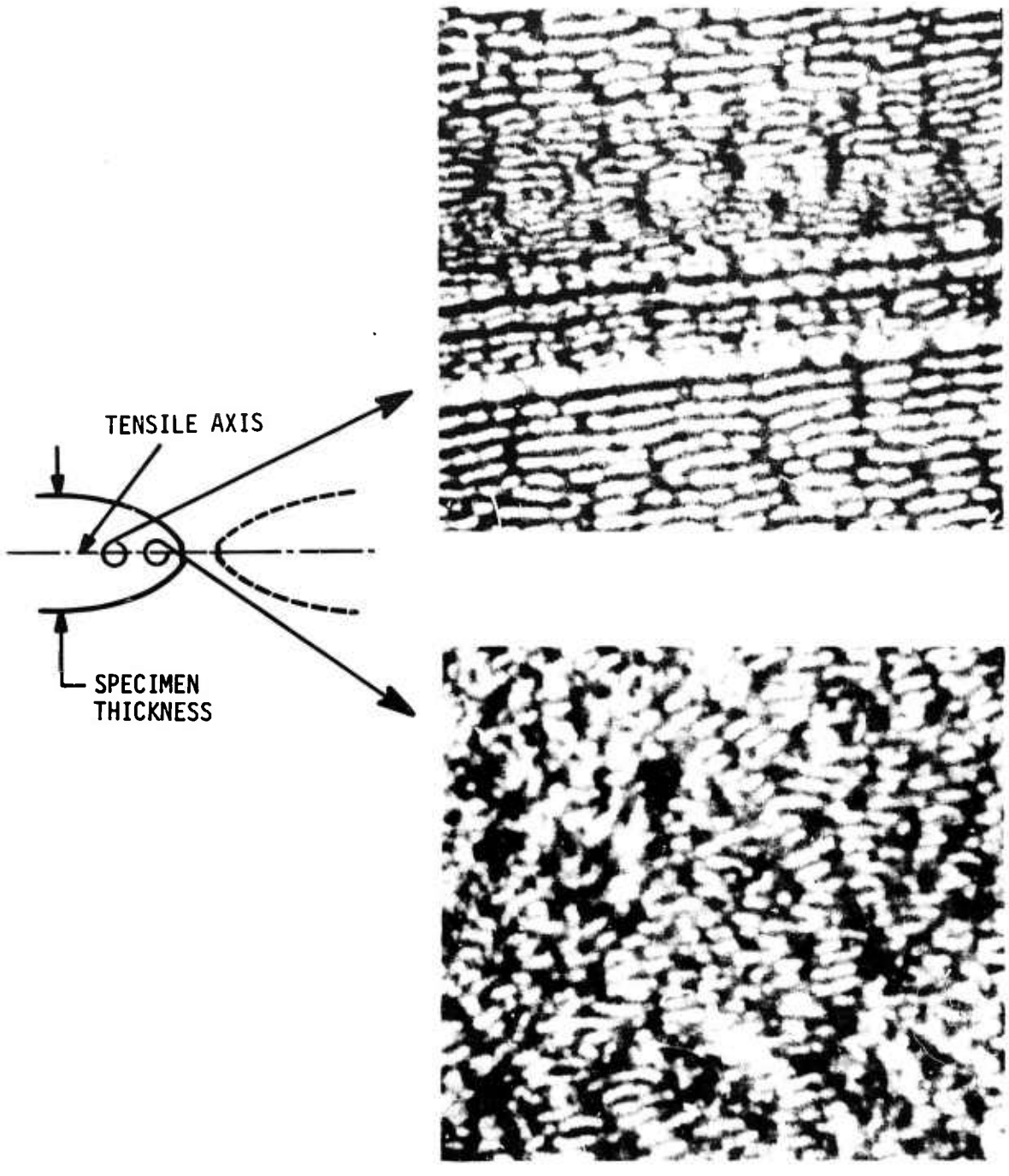

FIGURE 12. Breakup of NiAl Layers During Deformation (Necking) at 300°C. The dependence of the breakup on the overall reduction in area is apparent. 2000X.

Deposit 17

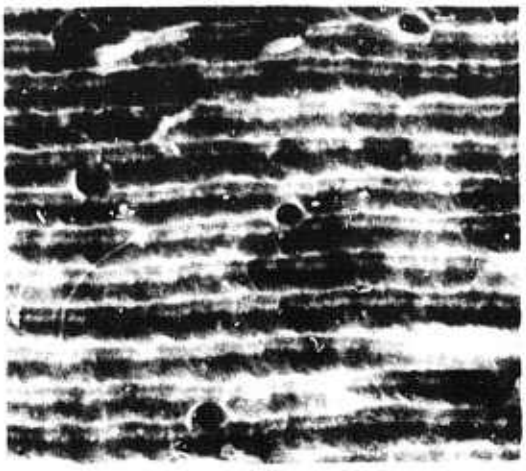

Deposit 18

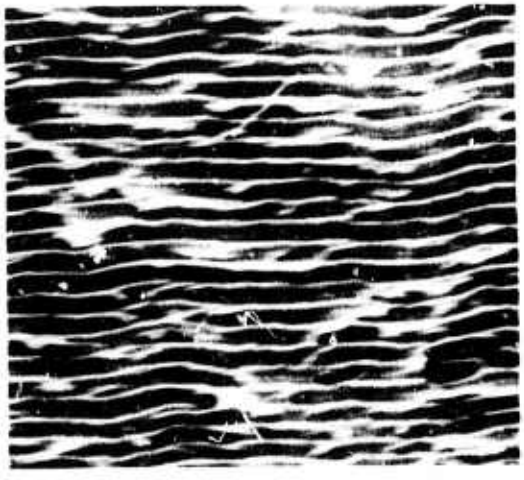

Deposit 19

Deposit 24

FIGURE 13. Microstructure of Al-NiAl Lamellar Composites, Obtained from Room Temperature Fracture Surfaces by SEM. Ductile behavior of the aluminum layers is most pronounced in Deposit 17, as indicated by chisel-point fractures (arrow). 4000X.

The microstructures of the Al-$TiAl_3$ composites are shown in Figure 14. The intermetallic layers are visible as light grey bands between the white lines, which are the chisel-point fractures of the aluminum layers. The major difference between these fracture surfaces is the greater roughness of Deposit 22. This roughness does not appear to be related to a translayer columnar structure and may instead reflect crack branching. Again, no delamination of the layers was observed.

The aluminum-beryllium microstructures are shown in Figure 15. The finer lamellar structure and higher percent reinforcement of Deposit 25 are presumed responsible for the more brittle appearance of the fracture. The appearance is related to the higher strength and lower elongation observed in the tensile tests, Table 9.

The fracture surfaces of the specimens tensile tested at 300°C are shown in Figure 16. The necking of the Al-Ni specimens is evident in Figure 16a; in this case the reduction in area was ∿97%. The layer structure is not visible on the fracture surface, Figure 16b, but has been illustrated in Figure 12. The Al-Ti fracture surface appearance, Figure 16c, is similar to that obtained in room temperature tests in spite of the much greater elongation observed at 300°C (1.8% versus 0.6%). Although the lamellar structure is not visible for the Al-Be sample, Figure 16d, examination of a portion of this sample away from the fracture surface indicated that the layers were in fact still present.

Compound Identification

In the Al-NiAl system, x-ray diffraction indicated that the desired $NiAl_3$ compound was obtained, although several diffraction peaks not indexable to this compound were observed. The compound identification results with the Al-TiAl system were inconclusive.

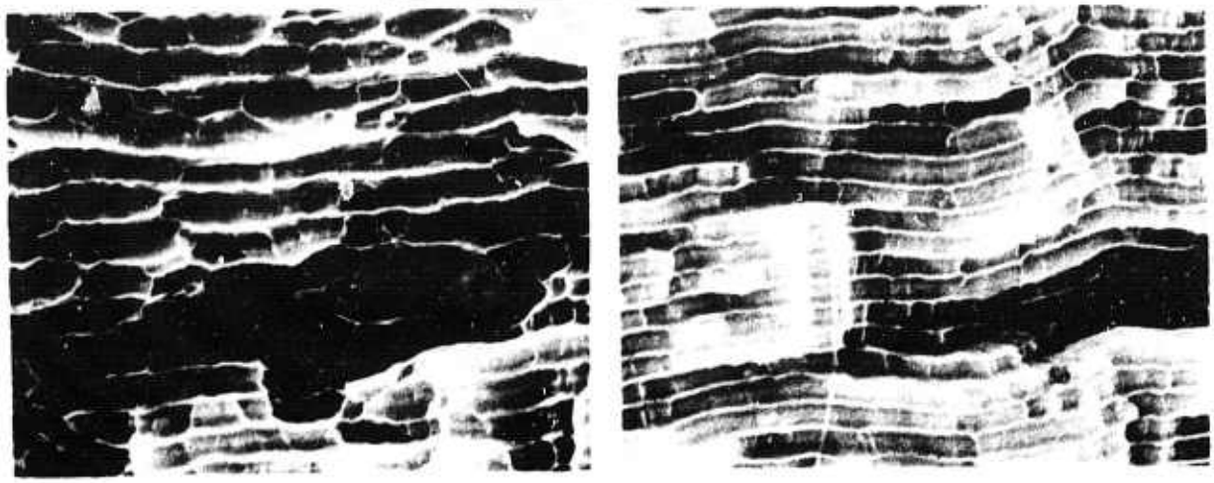

Deposit 20

Deposit 21

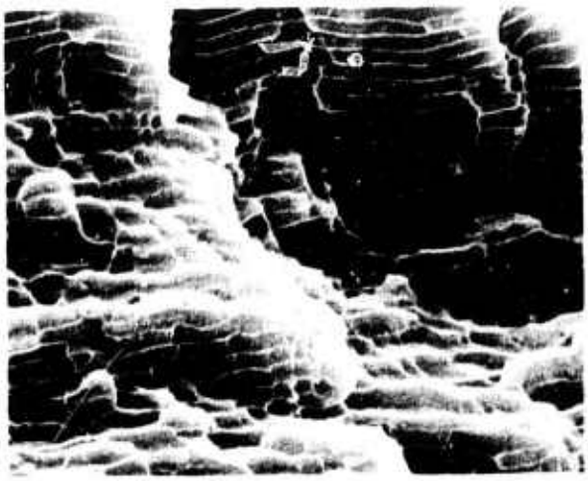

Deposit 22

FIGURE 14. Microstructure of Al-TiAl Lamellar Composites, Obtained from Room Temperature Fracture Surfaces by SEM. Crack branching is believed to be responsible for the surface roughness in Deposit 22. 4000X.

Deposit 23

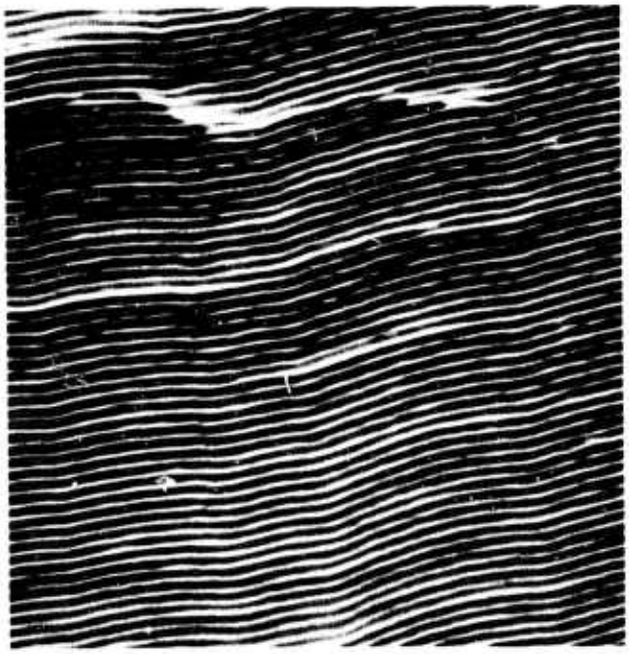

Deposit 25

FIGURE 15. Microstructure of Al-Be Lamellar Composites, Obtained from Room Temperature Fracture Surfaces by SEM. Smooth planar surface of Deposit 25 reflects the more brittle behavior of this specimen. 4000X.

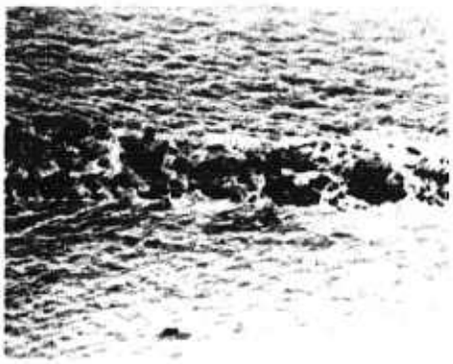

a. Fracture Surface Across Center of Photo, 400X.

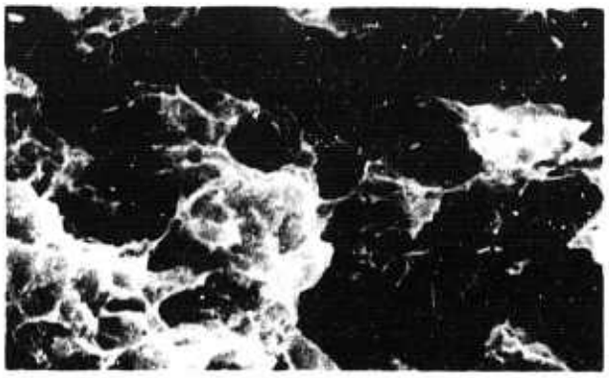

b. Fracture Surface at 4000X.

Al-NiAl Composite. Note high reduction in area and apparent absence of layer structure.

c. Al-TiAl Composite. Similar appearance to room temperature fracture surface, 4000X.

d. Al-Be Composite. Layer structure not apparent in the fracture surface but see text, 4000X.

FIGURE 16. Fracture Surfaces of Lamellar Composites Tensile Tested at 300° in Argon

CONSIDERATION OF ENGINEERING MATERIAL SYSTEMS APPROPRIATE TO DEPARTMENT OF DEFENSE NEEDS

BACKGROUND

Results of the first 2 years of research have demonstrated the validity of the lamellar composite concept. It was decided, therefore, to direct the third year of research towards the application of this concept to existing DOD materials problems. Advice on the nature of problems amenable to solution with lamellar composite technology was sought from personnel at the Air Force Materials Laboratory (AFML), the Air Force Aero Propulsion Laboratory (AFAPL), and NASA-Lewis. The problem identified that appears to have the greatest anticipated benefit from the use of sputter-deposited lamellar composites is obtaining improvement in the high temperature mechanical properties and oxidation resistance of turbine blade materials. This familiar problem has been, and remains, the limiting factor in improving gas turbine performance. The significance of the turbine blade material problem is increased by the anticipation that the generation of aircraft now in or entering service must be kept in service for about 10 years, due to political and economic factors. Improved turbine performance then becomes a major path to increased aircraft performance.

In the following sections consideration will be given to the utilization of lamellar composite technology to uniquely provide both the improvement in mechanical properties and oxidation protection required in high temperature turbine blade materials.

DEVELOPMENT OF MATERIALS CONCEPT

With respect to current technology, turbine blade metal temperatures obtainable with conventional superalloy metallurgy and coating systems are limited to ~980°C (1800°F). Further, the potential of refractory metals is limited by the fact that upon failure of coating systems that have been applied to date the refractory metal catastrophically oxidizes. Consideration of this information, then, leads to the postulation of a materials concept based on the unique capabilities of lamellar composites technolog

Briefly, it is felt that the high temperature strength properties of refractory metals can be utilized in combination with materials that can provide intrinsic protection from oxidation during service. A layered or lamellar structure is visualized, with one layer providing the strengthening and the alternate layer providing the intrinsic oxidation protection.

The previous work in this contract provides the support for the claim about strengthening. The retention of mechanical properties was observed to temperatures significantly higher than 0.6 of the absolute melting point (Tm) in the sputter-deposited lamellar composites produced. In addition, microstructural stability has been observed up to 0.6 Tm. In view of these properties of sputtered lamellar composites it is appropriate to consider a goal of developing a 1370°C (2500°F) turbine blade material. To withstand a metal temperature of 1370°C with a two-phase lamellar composite, the lower melting phase should have a melting point of 2467°C (4472°F), based on 0.6 Tm. Although we are aware of no two-phase system meeting this specification, at least three systems do approach it and therefore offer promise of desirable mechanical properties at temperatures near 1370°C.

The three systems considered practical for turbine blade application at metal temperatures near 1370°C on the basis of mechanical considerations and oxidation resistance are, in order of decreasing melting temperatures, as follows: W-W_2Zr, Nb-Nb_3Al and Mo-Mo_2Zr. In each case the entire lamellar airfoil structure would consist of alternate layers of a refractory metal and an intermetallic compound.

Concerning oxidation resistance, it was felt that it would be provided by a thin adherent surface scale of zirconia (ZrO_2) or alumina (Al_2O_3). This oxide scale would be generated by oxidation of the refractory intermetallics W_2Zr, Nb_3Al, or Mo_2Zr which would act as reservoirs to replenish the zirconia or alumina forming during exposure at temperature. During service, when an intermetallic compound layer has been either consumed or eroded away, the exposed refractory metal layer is expected to rapidly oxidize, thereby exposing a fresh oxidation-resistant intermetallic layer.

DISCUSSION OF POTENTIAL TURBINE BLADE MATERIAL SYSTEMS

For the W-W_2Zr system, the melting point of W_2Zr is 2150°C (3900°F) and the solubility of zirconium in tungsten at 1370°C (2500°F) is less than 1%. These characteristics are expected to provide a stable lamellar composite material. The W layers would contain small quantities of thoria, yttria, or HfC + C to stabilize the grain structure. The W_2Zr layers would contain yttrium to promote adherence and stability of the protective zirconia surface scale expected to form under service conditions.

In the Nb-Nb_3Al system, the melting point of Nb_3Al is 1950°C (3450°F). The homogeneity range of the compound and the solubility of aluminum in niobium are both significantly larger than in the above system, possibly indicating a lower degree of stability. The density, however, is only approximately 45% of the tungsten base system, which proportionately reduces the stress in rotating components. This system would also contain an oxide of hafnium, thorium or yttrium in the niobium layer and yttrium alloying additions in the Nb_3Al layer. An advantage of this system is the close expansivity matching between the base material and the protective alumina forming in service.

The Mo-Mo_2Zr system is very similar to the W-W_2Zr system except that the melting point of Mo_2Zr is only 1880°C (3416°F). The same grain-size stabilizing materials would be used in this system as in the W-W_2Zr system, with particular attention being focused on HfC + C additions.

EXPERIMENTAL APPROACH

Preliminary Evaluation

Initial material development activity would involve sputter deposition of the intermetallic compounds (W_2Zr, Nb_3Al, Mo_2Zr, etc.) in coupon form for evaluation of their oxidation behavior. In the lamellar systems, these compound layers are intended to provide the systems' oxidation resistance through formation of zirconia and alumina scales. The oxidation behavior would be determined by still-air weight-loss measurements. It is expected

that the sputtering experiments will also determine the sputtering yield behavior of the elements in combination, which will permit the design of the targets for the larger scale depositions.

A system or systems would then be selected as candidates for blade fabrication. Lamellar composites of these systems would be sputter deposited for metallurgical evaluation, including measurement of structural stability, composite oxidation behavior, stress rupture and burner rig testing. These specimens would be formed in tubular geometry in the apparatus being developed in the parallel effort to avoid edge effects (e.g., exposure of the refractory metals layers). Two extremes of layer pair thickness and two relative compound layer thicknesses would be employed to vary the physical properties of the composites. The remaining deposition parameters would be maintained constant.

Turbine Blade Fabrication by Sputtering

Hollow thin-walled turbine blade shapes with lamellar composite structure, as shown in Figure 17, would be a convenient configuration to produce by high-rate sputter deposition. Discussions with personnel at AFML and AFAPL revealed that similar configurations are currently being fabricated for testing and evaluation. The consensus was that the thin-wall concept would be satisfactory from a mechanical (e.g., stress) viewpoint. Some control of the flow of cooling air, i.e., an internal structure, such as an impingement tube, was thought to be required. This structure could readily be incorporated in the blade mandrel. Potential methods for attachment of the airfoil to the fir tree include brazing, bicasting and sputter-bonding. The sputter-bonding method would take advantage of the high-bond strength obtainable by sputter deposition to bond the airfoil shape to a permanent section of the mandrel during deposition. Other lamellar composite blade design concepts, including nonperforated shapes and shapes with exhaust slits in the blade tip, were discussed with Air Force personnel and were received with considerable interest.

In the fabrication approach visualized, modifications would be made to existing hardware to permit the sputter deposition of lamellar composites

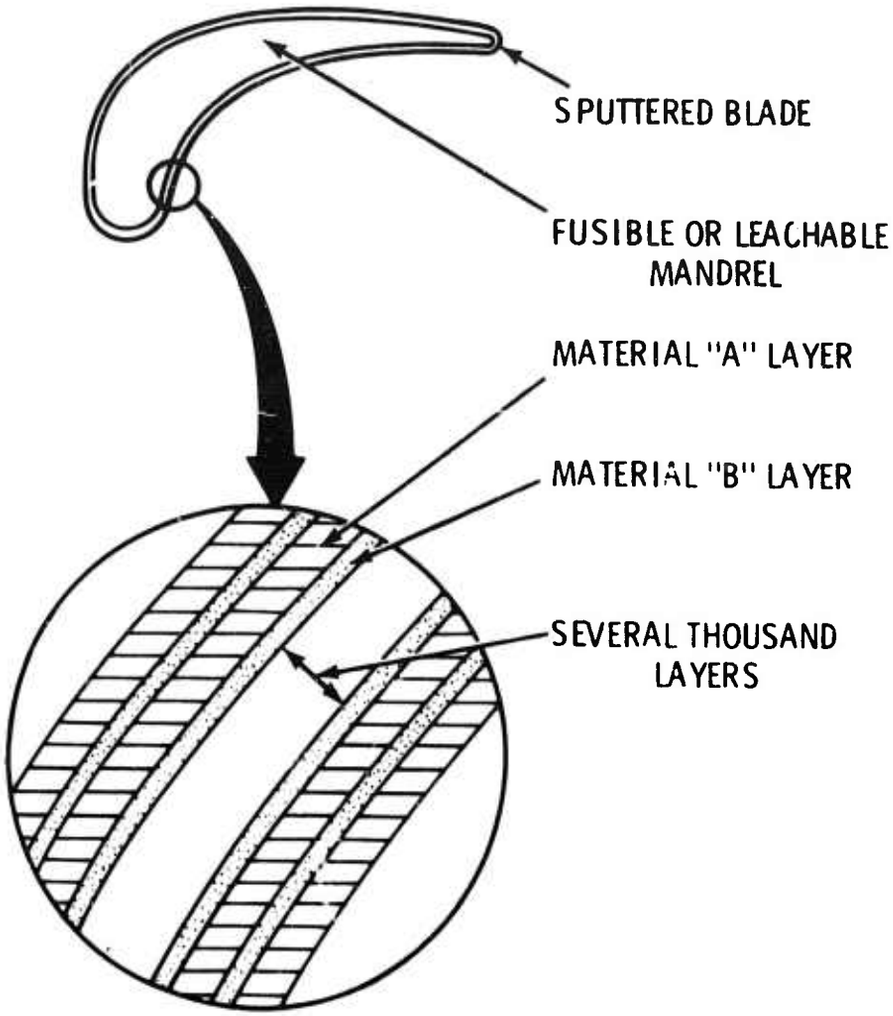

FIGURE 17. Cross-Section of Thin Lamellar Composite Turbine Blade Showing Alternate Layers of Repeating Thickness

in tubular test specimen and airfoil shapes. The material would be deposited on fusible or leachable mandrels. The mandrels revolve around split cylindrical targets at a rate calculated to produce the desired layer pair thickness, Figure 18. An appropriate number of airfoil shapes would be produced using the material systems selected.

FEATURES OF FABRICATION BY SPUTTER DEPOSITION

Sputter deposition offers the freedom to produce such material systems and shapes as identified above which employ intrinsic coating systems to

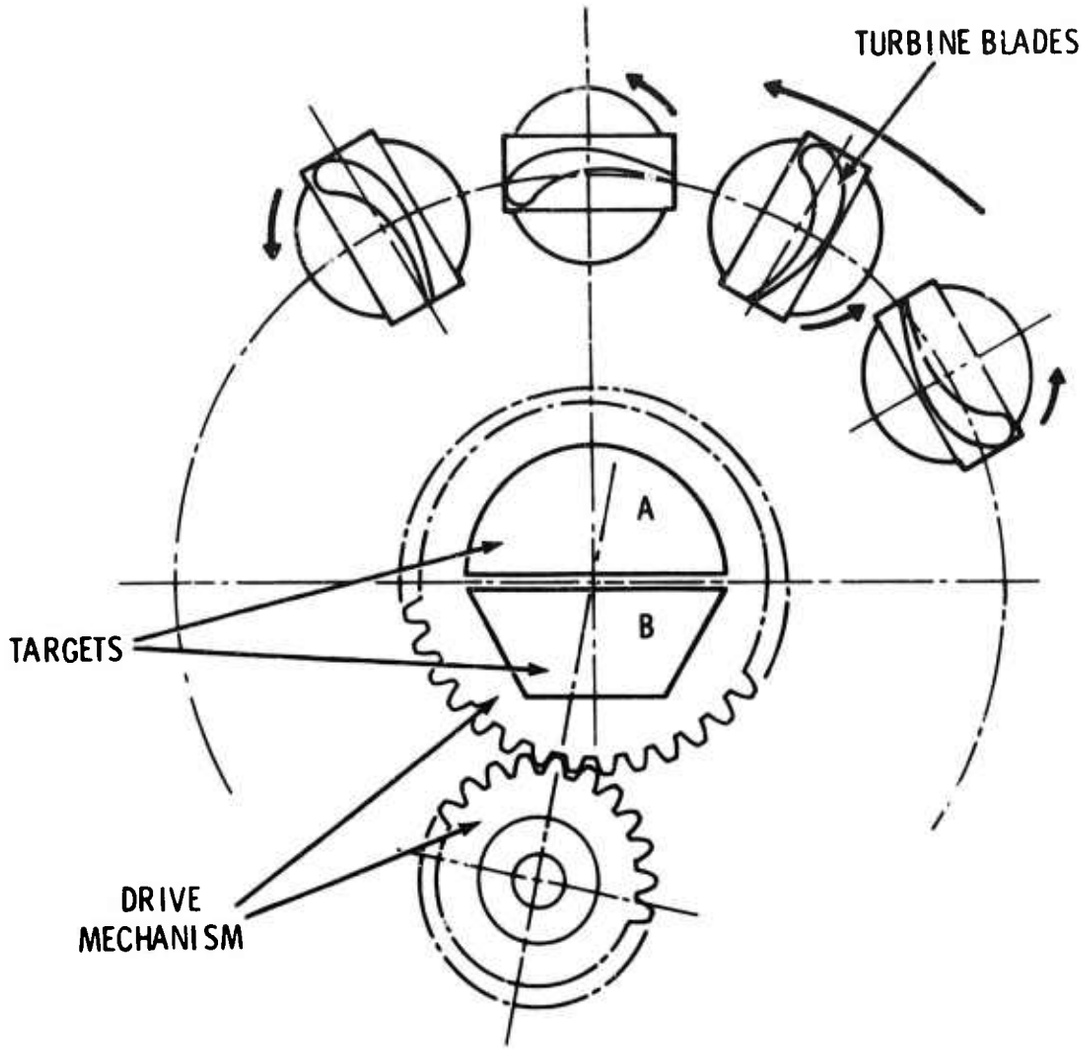

FIGURE 18. Rotation and Precession of Turbine Blades During Fabrication

protect refractory metals. In addition, sputtering's ability to produce graded layer thicknesses and, therefore, graded thermal or mechanical properties, or both, through the wall thickness of a blade may permit higher operating loads and/or temperatures, Figure 19. From a blade fabrication standpoint, the high cost of blades produced by conventional processing indicates that blade fabrication by sputter deposition may offer economic, as well as property, advantages. With sputter deposition, the ability to combine the material production, blade fabrication and coating into a single

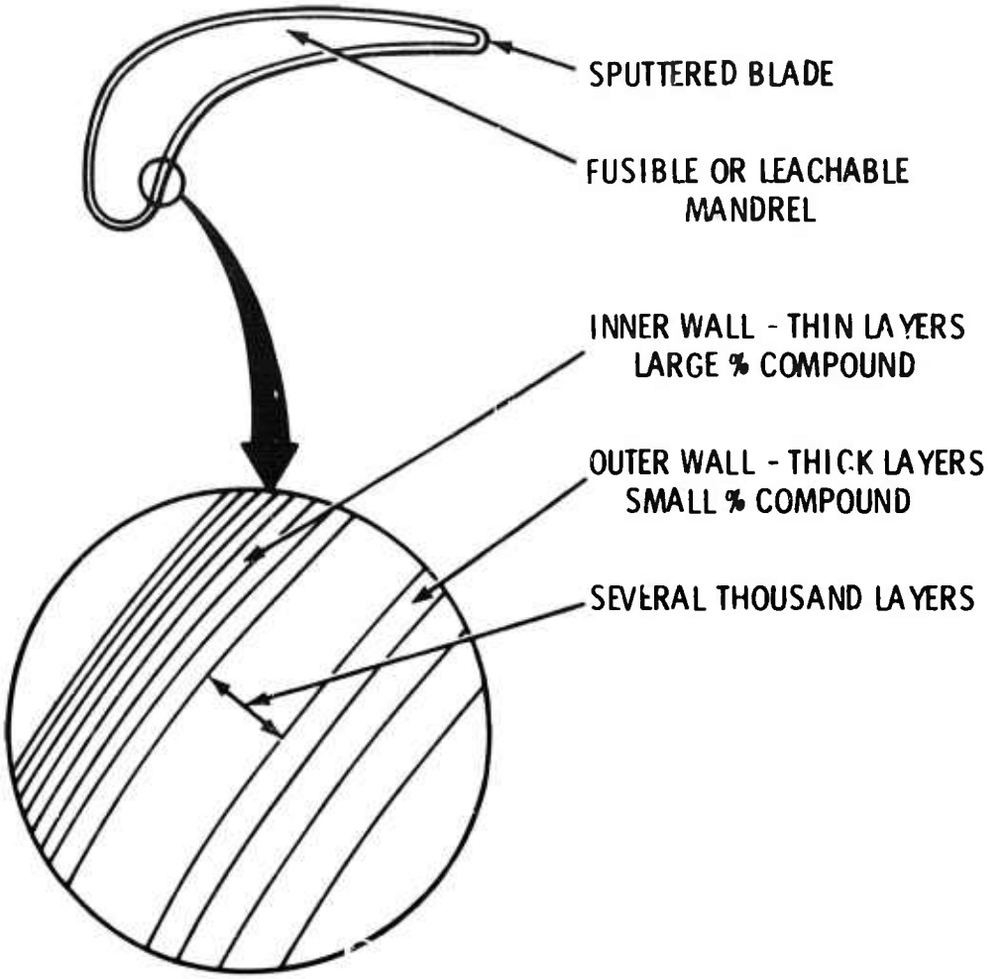

FIGURE 19. Cross-Section of Thin Lamellar Composite Turbine Blade Showing Layer Thickness Grading

operation is expected to result in per airfoil costs of $100 to $200. Costs for materials, mandrels, fir tree and attachment method, etc., would add to the airfoil fabrication cost.

ACKNOWLEDGEMENT

The authors are grateful to numerous members of Department staff for performance of the sputter deposition, metallography, and property testing.

REFERENCES

1. J. S. Koehler, Phys. Rev. B., 547 (1970).

2. W. A. Jesser and J. W. Mathews, Phil. Mag., 15, 1097 (1967).

3. W. A. Jesser and J. W. Mathews, Phil. Mag., 17, 475 (1968).

4. J. W. Mathews and W. A. Jesser, Phil. Mag., 20, 999 (1969).

5. H. R. Gardner, R. A. Busch and J. W. Patten, "Lamellar Composites Formed by Sputter Deposition," Semiannual Technical Report, December 1973, Sponsored by Advanced Research Projects Agency, Contract No. F44620-73-C-0071, ARPA Order No. 2482, Program Code No. 3D10, Battelle Northwest Laboratories, Richland, Washington.

6. H. R. Gardner, R. A. Busch and J. W. Patten, "Lamellar Composites Formed by Sputter Deposition," Annual Technical Report, June 1974, Sponsored by Advanced Research Projects Agency, Contract No. F44620-73-C-0071, Modification P00003, July 8, 1974, ARPA Order No. 2482, Program Code No. 3D10, Battelle Northwest Laboratories, Richland, Washington.

7. R. D. Nelson, Density Determinations of Plutonium, USAEC Report HW-80841, Hanford Atomic Products Operation, General Electric Co., February 1964.

8. R. D. Nelson, C. C. Land and F. H. Ellinger, Plutonium Handbook, Pacific Northwest Laboratories, Battelle Memorial Institute, Gordon and Breach Science Publishers, New York, 1967, edited by O. J. Wick, p. 320.

9. H. Mayer, Phil. Mag., 16, 594 (1933).

10. H. Sporn, Z. Physik., 112, 278 (1939).

11. R. V. Stuart, G. H. Wehner and G. S. Anderson, J. Appl. Phys., 40, 8031 (1969); J. Appl. Phys., 35, 1819 (1964).

12. P. S. Aggarwal and A. Goswami, Proc. Phys. Soc. (London), 70B, 708 (1957).

13. K. L. Chopra, M. R. Randlett and R. H. Duff, Phil. Mag., 16, 261 (1967).

14. P. N. Denbigh and R. B. Marcus, J. Appl. Phys., 37, 4325 (1966).

15. J. R. Bosnel and U. C. Voisey, Thin Solid Films, 6, 107 (1970).

16. G. Pilkington, G. Antwi-Boateng and G. Meyrick, Phase Transformations in Vapor-Quenched Molybdenum and Molybdenum-Gold Alloys, report AD-776970, Ohio State Univ. Research Foundation, Columbus, Ohio, 1974.

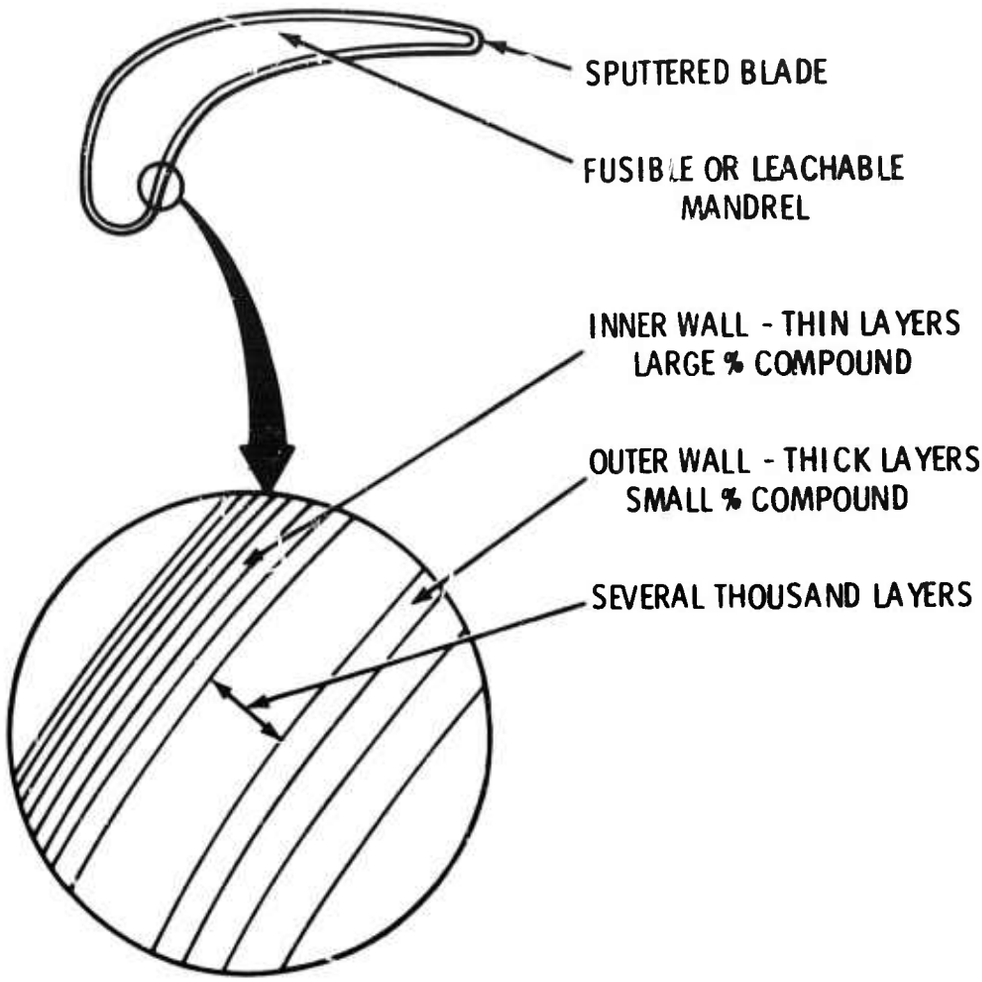

FIGURE 19. Cross-Section of Thin Lamellar Composite Turbine Blade Showing Layer Thickness Grading

operation is expected to result in per airfoil costs of $100 to $200. Costs for materials, mandrels, fir tree and attachment method, etc., would add to the airfoil fabrication cost.

ACKNOWLEDGEMENT

The authors are grateful to numerous members of Department staff for performance of the sputter deposition, metallography, and property testing.

REFERENCES

1. J. S. Koehler, Phys. Rev. B., 547 (1970).

2. W. A. Jesser and J. W. Mathews, Phil. Mag., 15, 1097 (1967).

3. W. A. Jesser and J. W. Mathews, Phil. Mag., 17, 475 (1968).

4. J. W. Mathews and W. A. Jesser, Phil. Mag., 20, 999 (1969).

5. H. R. Gardner, R. A. Busch and J. W. Patten, "Lamellar Composites Formed by Sputter Deposition," Semiannual Technical Report, December 1973, Sponsored by Advanced Research Projects Agency, Contract No. F44620-73-C-0071, ARPA Order No. 2482, Program Code No. 3D10, Battelle Northwest Laboratories, Richland, Washington.

6. H. R. Gardner, R. A. Busch and J. W. Patten, "Lamellar Composites Formed by Sputter Deposition," Annual Technical Report, June 1974, Sponsored by Advanced Research Projects Agency, Contract No. F44620-73-C-0071, Modification P00003, July 8, 1974, ARPA Order No. 2482, Program Code No. 3D10, Battelle Northwest Laboratories, Richland, Washington.

7. R. D. Nelson, Density Determinations of Plutonium, USAEC Report HW-80841, Hanford Atomic Products Operation, General Electric Co., February 1964.

8. R. D. Nelson, C. C. Land and F. H. Ellinger, Plutonium Handbook, Pacific Northwest Laboratories, Battelle Memorial Institute, Gordon and Breach Science Publishers, New York, 1967, edited by O. J. Wick, p. 320.

9. H. Mayer, Phil. Mag., 16, 594 (1933).

10. H. Sporn, Z. Physik., 112, 278 (1939).

11. R. V. Stuart, G. H. Wehner and G. S. Anderson, J. Appl. Phys., 40, 8031 (1969); J. Appl. Phys., 35, 1819 (1964).

12. P. S. Aggarwal and A. Goswami, Proc. Phys. Soc. (London), 70B, 708 (1957).

13. K. L. Chopra, M. R. Randlett and R. H. Duff, Phil. Mag., 16, 261 (1967).

14. P. N. Denbigh and R. B. Marcus, J. Appl. Phys., 37, 4325 (1966).

15. J. R. Bosnel and U. C. Voisey, Thin Solid Films, 6, 107 (1970).

16. G. Pilkington, G. Antwi-Boateng and G. Meyrick, Phase Transformations in Vapor-Quenched Molybdenum and Molybdenum-Gold Alloys, Report AD-776970, Ohio State Univ. Research Foundation, Columbus, Ohio, 1974.

REFERENCES (contd)

17. A. Mattiessen and C. Vogt, Anv. Phys. Chem. (Pogg), 122, 19 (1864).

18. V. S. Kopan and A. V. Lysenko, Fiz. Metal. Metalloved., 29, 1074 (1970).

19. J. K. Stanley, Electrical and Magnetic Properties of Metals, ASM, Metals Park, Ohio, 1963, Chapter 2.

20. P. W. Bridgeman, Proc. Am. Acad. Arts, 81, 165 (1952).

21. G. H. Wehner and G. S. Anderson, Handbook of Thin Film Technology, McGraw-Hill Book Co., New York, 1970, edited by L. J. Maissel and R. Glang, Chapter 3.

22. A. W. Overhauser and R. L. Gorman, Phys. Rev., 102, 676 (1956).

23. K. Fuchs, Proc. Cambridge Phil. Soc., 34, 100 (1938).

24. A. F. Mayades and M. Shatzkes, Phys. Rev. B, 1, 1382 (1970).

25. E. E. Mola and J. M. Heras, Thin Solid Films, 18, 137 (1973).

26. F. W. Reynolds and G. R. Stilwell, Phys. Rev., 88, 418 (1952).

27. G. Tammann and K. L. Dreyer, Ann. Physik, 16, 111 (1933).

28. A. F. Trotman-Dickenson, Gas Kinetics, Butterworth, London, 1955, Chapter 2.

29. G. K. Wehner, General Mills Report 2309, 1962.

30. D. Gatchley, Met. Rev., 10, 79 (1965).

31. W. H. Lawson and H. W. Kerr, Met. Trans., 2, 2853 (1971).

32. Y. G. Nakagawa and G. C. Weatherly, Acta Met., 20, 345 (1971).

33. A. Kelly and G. J. Davies, Met. Rev., 10, 1 (1965).

34. H. E. Cline and D. Lee, Acta Met., 18, 315 (1970).

35. D. A. Koss and S. M. Copley, Met. Trans., 2, 1557 (1971).

36. E. R. Thompson and F. D. Lemkey, Trans. ASM, 62, 140 (1969).

37. R. T. Quinn, R. W. Kraft and R. W. Hertzberg, Trans. ASM, 62, 38 (1969).

APPENDIX I

TEMPERATURE CORRECTION OF RESISTIVITY DATA

Accurate determination of activation energies from the Arrhenius relation requires that the reaction rate, i.e., the time rate of change of resistivity $\Delta\rho/\Delta t$, be determined for similar structures. In an attempt to do this a temperature coefficient of resistivity was assumed and measured resistivity values were first corrected to the maximum temperature reached by the specimen during that specific resistivity experiment and then corrected to 982°C. Results of these calculations, presented in Tables I-1 to I-8, must be viewed with caution, however. Temperature corrections to resistivity data are usually made using the relationship $\rho_2 = \rho_1 + \alpha\rho_1 (T_2 - T_1)$, where α is the temperature coefficient of resistivity and ρ_1 and ρ_2 are resistivities at temperatures T_1 and T_2, respectively.[I-1] However, if resistivity is approximately linear with temperature above the Debye temperature, as is generally true,[I-1] then the temperature coefficient α as defined above must also be a function of temperature. It has been shown, in fact, that α is a linear function of conductivity for Cu[I-2] and it is, therefore, a linear function of temperature. If, however, the values of ρ and α are measured at one temperature and held constant, the relation $\rho_2 = \rho_1 = \rho_1 + \alpha_{25}\rho_{25} (T_2 - T_1)$ should be valid, where α_{25} and ρ_{25} are measured at 25°C in this case. This approach was used for correcting resistivity data in this investigation using $\alpha = 0.00393/°C$, which is typical of pure Cu.[I-3] Here ρ_{25} was measured after heat treatment for each resistivity experiment. This is not a very accurate approximation because, although temperature coefficients are nearly identical for most pure metals,[I-1] current thin film resistivity theory[I-4-I-6] predicts decreasing values of α for decreasing film (or layer) thickness. It is possible to calculate values of α for any resistance-temperature data, of course, and this was done for the longest heat treatment at each temperature. Results are displayed in Figure I-1 and the range of values corresponds very well to published data for bulk Cu.[I-3] Also note that α for annealed

structures here approaches the bulk value. Using the above approach, however, it is not possible to separate residual resistivity and temperature-effect resistivity contributions.

Note that in Tables I-1 to I-8 the room temperature resistivities as corrected to 982°C differ widely. This resulted from the use of resistivities measured at 25°C after each heat treatment to generate the temperature corrections. The one exception to this practice was the 330°C data (Table I-8). These data were corrected to 982°C using a mean 25°C resistivity from the other experiments because time at temperature to substantially lower the 25°C resistivity would have been excessive and, therefore, the experiment was not carried out to large reductions in resistivity. The approximation is better for longer times at temperature, as is demonstrated by increasing resistivity (corrected to 982°C) with decreasing temperature for times near 100 min. Further, data obtained at temperatures of 750°C or above approached the same resistivity limit at about 100 min, as would be expected from TEM observations of the spheroidized structure. Samples heat treated at 650°C and below were observed to retain the layered structure or very fine sphere size and were expected to retain higher resistivities as was also observed. The 330°C data were excluded from these comparisons because of the manner in which they were corrected and the 976°C data (specimen TCC-2) were excluded because they were measured on a sample taken from a different sputter deposition experiment.

Small variations in resistivity after long times at temperature are believed to have resulted from degradation in the thermocouple and/or resistivity lead attachments welded to the samples. The irregularities during the first minutes at temperature resulted from inability of the zirconia bath material to behave in a completely fluid manner and remain at constant temperature in the vicinity of the sample during sample heating

TABLE I-1. Resistivity of OTLC-2 to 982°C

Corrected Time (min)	T (°C)	ρ (μΩ cm)	(982°C -T)	$\rho_{982^{o}C}$
0	38	14.28	944	27.52
.1	38	14.24	944	27.48
.2	38	14.26	944	27.50
.3	38	14.26	944	27.50
.4	409	81.96	573	90.00
.5	940	27.49	42	28.08
.6	953	24.16	29	24.57
.7	973	19.27	9	19.40
.8	970	19.78	12	19.95
.9	969	18.96	13	19.14
1.0	967	19.27	15	19.48
1.1	966	19.33	16	19.55
1.2	966	19.19	16	19.41
1.3	965	19.09	17	19.33
2.3	966	18.33	16	18.55
3.3	968	17.82	14	18.02
4.3	969	17.46	13	17.64
5.3	971	17.14	11	17.29
6.3	973	16.96	9	17.09
7.3	973	16.87	9	17.00
8.3	974	16.73	8	16.84
9.3	976	16.60	6	16.68
10.3	976	16.47	6	16.55
11.3	977	16.35	5	16.42
12.3	978	16.27	4	16.33
13.3	979	16.18	3	16.22
14.3	979	16.13	3	16.17
15.3	979	16.07	3	16.11
16.3	980	16.02	2	16.05
17.3	980	15.98	2	16.01
18.3	981	15.95	1	15.96
19.3	981	15.92	1	15.93
20.3	981	15.88	1	15.89
25.3	982	15.73	0	15.73
30.3	982	15.65	0	15.65
35.3	982	15.63	0	15.63
40.3	982	15.64	0	15.64
45.3	982	15.61	0	15.61
50.3	979	15.56	3	15.60
55.3	976	15.52	6	15.60
∞	25	3.57[a]	957	17.00
∞	-196	.95[a]		

a. Measured after elevated temperature resistivity determination.

TABLE I-2. Resistivity of TLC-2 to 976°C

Corrected Time (min)	T (°C)	ρ (μΩ cm)	(976°C -T)	$\rho_{976°C}$	(982°C -T)	$\rho_{982°C}$
0	32	22.10	944	39.67	950	39.87
.1	35	22.28	941	39.88	947	40.00
.2	49	22.29	927	39.63	933	39.74
.3	149	23.75	827	39.22	833	39.33
.4	890	29.91	86	31.52	92	31.63
.5	884	26.59	92	28.31	98	28.42
.6	916	24.56	60	25.68	66	25.79
.7	923	22.90	53	23.89	59	24.00
.8	917	22.68	59	23.78	65	23.90
.9	913	22.36	63	23.54	69	23.65
1.0	913	22.21	63	23.39	69	23.50
1.1	910	22.01	66	23.24	72	23.36
1.2	908	21.88	68	23.15	74	23.26
1.3	908	21.75	68	23.02	74	23.13
2.3	910	21.07	66	22.30	72	22.42
3.3	917	20.68	59	21.78	65	21.90
4.3	922	20.39	54	21.40	60	21.51
5.3	928	20.21	48	21.11	54	21.22
8.7	944	19.87	32	20.47	38	20.58
9.7	947	19.82	29	20.36	35	20.47
10.7	950	19.74	26	20.23	32	20.34
11.7	955	19.72	21	20.11	27	20.23
12.7	955	19.65	21	20.04	27	20.16
13.7	958	19.63	18	19.97	24	20.08
14.7	960	19.61	16	19.91	22	20.02
15.7	960	19.57	16	19.87	22	19.98
16.7	962	19.50	14	19.76	20	19.87
17.7	964	19.54	12	19.76	18	19.88
18.7	965	19.52	11	19.73	17	19.84
19.7	966	19.47	10	19.66	16	19.77
20.7	967	19.47	9	19.64	15	19.75
21.7	968	19.48	8	19.63	14	19.74
22.7	969	19.43	7	19.56	13	19.67
27.7	972	19.39	6	19.50	12	19.61
32.7	973	19.33	3	19.39	9	19.50
37.7	974	19.27	2	19.31	8	19.42
42.7	975	19.24	1	19.26	7	19.37
47.7	975	19.23	1	19.25	7	19.36
52.7	976	19.17	0	19.17	6	19.28
57.7	976	19.15	0	19.15	6	19.26
62.7	976	19.14	0	19.14	6	19.25
67.7	976	19.10	0	19.10	6	19.21
72.7	976	19.10	0	19.10	6	19.21
77.7	976	19.08	0	19.08	6	19.19
82.7	976	19.08	0	19.08	6	19.19
87.7	976	19.08	0	19.08	6	19.19
92.7	976	19.06	0	19.06	6	19.17
97.7	976	19.06	0	19.06	6	19.17
102.7	976	19.05	0	19.05	6	19.16
105.7	976	19.05	0	19.05	6	19.16
112.7	976	19.05	0	19.05	6	19.16
∞	25	4.76[a]	951	22.55	957	22.66
∞	196	1.26[a]				

a. See Table I-1.

TABLE I-3. Resistivity of OTLC-2 to 837°C

Corrected Time (min)	T (°C)	ρ (μΩ cm)	(837°C − T)	$\rho_{837°C}$	(982°C − T)	$\rho_{982°C}$
0	31	13.85	806	25.35	951	27.42
.1	31	13.87	806	25.37	951	27.44
.2	31	13.86	806	25.36	951	27.43
.3	31	13.86	806	25.36	951	27.43
.4	521	54.95	317	59.47	461	61.53
.5	818	25.58	19	25.85	164	27.92
.6	833	19.87	4	19.93	149	22.00
.7	834	18.96	3	19.00	148	21.07
.8	834	17.98	3	18.02	148	20.09
.9	833	18.00	4	18.06	149	20.13
1.0	833	18.29	4	18.35	149	20.42
1.1	833	18.60	4	18.60	149	20.73
1.2	815	18.67	22	18.98	167	21.05
1.3	818	16.12	19	16.39	164	18.46
2.3	818	16.08	19	16.35	164	18.42
3.3	818	15.72	19	15.99	164	18.06
4.3	820	15.46	17	15.70	162	17.77
5.3	821	15.26	16	15.49	161	17.56
6.3	822	15.12	15	15.33	160	17.40
7.3	824	14.99	13	15.18	158	17.24
8.3	825	14.67	12	15.04	157	17.11
9.3	827	14.77	10	14.91	155	16.98
10.3	828	14.70	9	14.83	154	16.90
11.3	828	14.60	9	14.73	154	16.80
12.3	829	14.53	8	14.64	153	16.71
13.3	830	14.48	7	14.58	152	16.65
14.3	830	14.43	7	14.53	152	16.60
15.3	830	14.38	7	14.48	152	16.55
16.3	831	14.34	6	14.43	151	16.49
17.3	832	14.32	5	14.39	150	16.46
18.3	832	14.26	5	14.33	150	16.40
19.3	832	14.24	5	14.31	150	16.38
20.3	833	14.20	4	14.26	149	16.33
25.3	834	14.07	3	14.11	148	16.18
29.8	835	13.97	2	14.00	147	16.07
30.3	835	14.00	2	14.03	147	16.10
36.3	835	13.91	2	13.94	147	16.01
42.3	836	13.82	1	13.83	146	15.90
48.3	837	13.76	0	13.76	145	15.83
54.3	837	13.67	0	13.67	145	15.74
60.3	837	13.63	0	13.63	145	15.70
∞	25	3.63[a]	812	15.21	957	17.28
∞	196	1.10[a]				

a. See Table I-1.

TABLE I-4. Resistivity of OTLC-2 to 754°C

Corrected Time (min)	T [°C]	ρ [μΩ cm]	(754°C	T]	$\rho_{754°C}$	1982°C	T]	$\rho_{982°C}$
0	31	11.73	723		22.74	951		26.22
.1	33	11.74	721		22.73	949		26.20
.2	33	11.75	721		22.74	949		26.21
.3	33	11.73	721		22.73	949		26.19
.4	277	16.46	477		23.77	705		27.20
.5	341	18.55	413		24.88	641		28.32
.6	656	20.95	90		22.45	326		25.92
.7	690	17.27	64		18.25	292		21.72
.8	701	16.46	53		17.27	281		20.74
.9	701	15.42	53		16.23	281		19.70
1.3	691	15.75	63		16.71	291		20.18
1.1	694	15.23	60		16.15	288		19.62
1.2	692	16.13	62		17.08	290		20.55
1.3	690	16.49	64		17.47	292		20.94
2.3	694	15.59	60		16.51	288		19.98
3.3	702	15.14	52		15.94	280		19.41
4.3	708	14.93	46		15.63	274		19.11
5.3	714	14.77	40		15.38	268		18.85
6.3	717	14.62	37		15.19	265		18.66
7.3	720	14.52	34		15.04	262		18.51
8.3	720	14.11	34		14.63	262		18.10
9.3	718	14.72	36		15.27	264		18.74
10.3	718	14.46	36		15.01	265		18.50
11.3	719	14.41	35		14.95	263		18.42
12.3	722	14.29	32		14.78	260		18.25
13.3	724	14.18	30		14.64	258		18.11
14.3	727	14.05	27		14.46	255		17.94
15.3	729	13.92	25		14.30	253		17.78
16.3	730	13.78	24		14.15	252		17.62
17.3	732	13.65	22		13.99	250		17.46
18.3	734	13.52	20		13.83	248		17.30
19.3	735	13.38	19		13.67	247		17.14
20.3	736	13.26	18		13.54	246		17.01
25.3	742	12.70	12		12.88	240		16.36
30.3	745	12.32	9		12.46	237		15.93
35.3	747	12.02	7		12.14	235		15.61
40.3	749	11.85	5		11.93	233		15.40
45.3	750	11.72	4		11.78	232		15.26
50.3	751	11.61	4		11.67	232		15.15
55.3	751	11.49	3		11.54	231		15.01
60.3	751	11.42	3		11.47	231		14.94
65.3	752	11.34	2		11.37	230		14.84
70.3	752	11.28	2		11.32	230		14.79
75.3	753	11.24	1		11.26	229		14.73
80.3	753	11.19	1		11.21	229		14.68
85.3	753	11.15	1		11.17	229		14.64
90.3	753	11.11	1		11.13	229		14.60
95.3	753	11.07	1		11.09	229		14.56
100.3	753	11.05	1		11.07	229		14.54
105.3	754	11.02	0		11.02	228		14.49
110.3	754	11.00	0		11.00	228		14.47
115.3	754	10.98	0		10.98	228		14.45
120.3	754	10.97	0		10.97	228		14.44
125.3	754	10.95	0		10.95	228		14.42
130.3	754	10.92	0		10.92	228		14.39
135.3	754	10.91	0		10.91	228		14.38
140.3	754	10.92	0		10.92	228		14.39
145.3	754	10.91	0		10.91	228		14.38
150.3	754	10.89	0		10.89	228		14.36
155.3	754	10.86	0		10.86	228		14.33
160.3	754	10.84	0		10.84	228		14.31
165.3	754	10.82	0		10.82	228		14.29
170.3	754	10.81	0		10.81	228		14.28
175.3	754	10.80	0		10.80	228		14.27
203.3	754	10.74	0		10.74	228		14.21
226.3	754	10.68	0		10.68	228		14.15
251.3	754	10.63	0		10.63	228		14.10
276.3	754	10.61	0		20.61	228		14.08
-	25	1.8775[a]	729		15.04	957		18.46
-	1906	1.560[a]						

a. See Table I-1.

TABLE I-5. Resistivity of OTLC-2 to 641°C

Corrected Time (min)	T (°C)	ρ (μΩ cm)	(641°C -T)	$\rho_{641°C}$	(982°C -T)	$\rho_{982°C}$
0	36	15.10	605	28.06	946	35.36
.1	36	15.13	605	28.09	946	35.39
.2	36	15.14	605	28.10	946	35.40
.3	36	15.14	605	28.10	946	35.40
.4	288	47.80	353	55.36	694	62.66
.5	554	27.99	87	29.85	428	37.17
.6	599	23.60	42	24.50	383	31.80
.7	618	20.94	23	21.43	364	28.74
.8	624	19.48	17	19.84	358	27.15
.9	625					
1.0	625	18.38	16	18.72	357	26.03
1.1	625	18.36	16	18.70	357	26.01
1.2	624	18.39	17	18.75	358	26.06
1.3	624	18.39	17	18.75	358	26.06
2.3	624	18.36	17	18.72	358	26.03
3.3	625	18.26	16	18.60	357	25.91
4.3	626	18.18	15	18.50	356	23.66
5.6	627	18.05	14	18.35	355	25.65
6.3	627	18.00	14	18.30	355	25.60
7.3	628	17.94	13	18.24	354	25.52
8.3	629	17.89	12	18.15	353	25.45
9.3	629	17.84	12	18.10	353	25.40
10.3	629	17.80	12	18.06	353	25.36
20.9	635	17.40	6	17.53	347	24.83
30.9	637	17.14	4	17.23	34[illegible]	24.53
40.9	638	16.90	3	16.96	344	24.27
50.9	639	16.71	2	16.75	343	24.06
60.9	639	16.55	2	16.59	343	23.90
70.9	640	16.40	1	16.42	342	23.72
84.9	641	16.20	0	16.20	341	23.50
94.9	641	16.08	0	16.08	341	23.38
104.9	641	15.90	0	15.90	341	23.20
124.9	641	15.63	0	15.63	341	22.93
154.9	640	15.25	0	15.22	342	22.57
174.9	640	15.02	0	15.04	342	22.34
204.9	641	14.69	0	14.69	341	21.99
254.9	641	14.25	0	14.25	341	21.55
304.9	641	13.90	0	13.90	341	21.20
354.9	641	13.65	0	13.65	341	20.95
404.9	641	13.43	0	13.43	341	20.73
454.9	641	13.28	0	13.28	341	20.58
504.9	641	13.15	0	13.15	341	20.45
554.9	641	13.04	0	13.04	341	20.34
604.9	641	12.98	0	12.98	341	20.28
654.9	641	12.90	0	12.90	341	20.20
704.9	641	12.83	0	12.83	341	20.13
754.9	641	12.77	0	12.77	341	20.07
804.9	641	12.71	0	12.71	341	20.01
854.9	641	12.64	0	12.64	341	19.94
904.9	641	12.71	0	12.71	341	20.01
∞	25	5.4495[a]	616	18.64	957	25.95
∞	165	2.677[a]				

a. See Table I-1.

TABLE I-6. Resistivity of OTLC-2 to 640°C

Corrected Time (min)	T (°C)	ρ (μΩ cm)	(640°C - T)	$\rho_{640°C}$	(982°C - T)	$\rho_{982°C}$
0	26	14.69	614	27.22	956	34.20
.1	26	14.7	614	27.23	956	34.21
.2	26	14.7	614	27.23	956	34.21
.3	88	15.9	552	27.18	894	34.17
.4	259	49.38	381	57.00	723	63.99
.5	445	41.01	195	45.01	537	52.00
.6	582	27.91	58	57.7	400	36.07
.7	629	20.92	11	21.14	353	28.12
.8	640	17.92	0	17.92	342	24.91
.9	633	16.54	7	16.67	349	23.66
1.0	626	15.49	14	15.77	356	22.76
1.1	624	16.15	16	16.50	358	23.40
1.2	622	16.42	18	16.79	360	23.78
1.3	622	16.33	18	16.70	360	23.69
2.3	621	16.76	19	17.15	361	24.13
3.3	621	16.79	19	17.18	361	24.17
4.3	621	16.72	19	17.15	361	24.14
5.6	621	16.69	19	17.09	361	24.07
6.3	621	16.66	19	17.05	361	24.04
7.3	621	16.62	19	17.02	361	24.01
8.3	621	16.59	19	16.98	361	23.97
9.3	621	16.57	19	16.96	361	23.94
10.3	621	16.52	19	16.91	361	23.90
20.9	621	16.25	19	16.64	361	23.62
30.9	620	16.03	20	16.43	362	23.42
40.9	620	15.83	20	16.24	362	23.22
50.9	620	15.67	20	16.07	362	23.06
60.9	620	15.51	20	15.91	362	22.89
70.9	620	15.34	20	15.75	362	22.73
84.9	620	15.12	20	15.53	362	22.52
94.9	620	15.04	20	15.44	362	22.43
104.9	620	14.89	20	15.30	362	22.29
124.9	620	14.59	20	15.00	362	21.98
154.9	619	14.19	21	14.61	363	21.60
174.9	619	13.96	21	14.39	363	21.38
204.9	620	13.63	20	14.04	362	21.03
254.9	621	13.23	19	13.61	361	20.60
289.6	622	13.02	18	13.38	360	20.37
354.9	622	12.70	18	13.08	360	20.06
384.6	622	12.59	18	12.97	360	19.95
484.9	623	12.03	17	12.65	359	19.63
529.6	623	12.22	17	12.57	359	19.56
574.9	623	12.15	17	12.50	359	19.49
619.6	623	12.09	17	12.44	359	19.43
654.9	623	17.03	17	12.38	359	19.36
709.9	623	11.97	17	12.33	359	19.31
754.9	623	11.93	17	12.38	359	19.27
844.9	622	11.85	18	12.21	360	19.20
934.9	622	11.80	18	12.17	360	19.16
979.6	622	11.75	18	12.12	360	19.11
∞	25	5.2[a]	615		957	
∞	196					

a. See Table I-1.

TABLE I-7. Resistivity of OTLC-2 to 550°C

Corrected Time (min)	T (°C)	ρ (μΩ cm)	(556°C -T)	$\rho_{556°C}$	(982°C -T)	$\rho_{982°C}$
0	28	14.58	528	34.96	954	51.40
.1	30	14.59	526	34.89	952	51.33
.3	31	14.58	525	34.84	951	51.28
.4	44	14.79	512	34.55	938	50.99
.6	491	23.41	65	25.92	491	42.36
.7	544	18.32	12	18.78	438	35.22
.8	550	16.91	6	17.14	432	33.58
1.0	546	16.46	10	16.85	436	33.29
1.1	545	16.45	11	16.87	437	33.31
1.3	545	16.69	11	17.11	437	33.55
2.3	544	16.85	12	17.31	438	33.75
3.3	545	16.83	11	17.25	437	33.69
4.3	545	16 79	11	17.21	437	33.65
5.3	546	16.77	10	17.16	436	33.60
6.3	547	16.74	9	17.09	435	33.53
7.3	548	16.71	8	17.02	434	33.46
8.3	549	16.69	7	16.96	433	33.40
9.5	550	16.63	6	16.86	432	33.30
10.1	550	16.60	6	16.83	432	33.27
10.8	551	16.58	5	16.77	431	33.21
11.5	551	16.59	5	16.78	431	33.22
12.1	551	16.57	5	16.76	431	33.20
12.8	551	16.58	5	16.77	431	33.21
14.1	552	16.55	4	16.70	430	33.14
14.8	552	16.52	4	16.67	430	33.11
16.1	552	16.51	4	16.66	430	33.10
16.8	553	16.49	3	16.61	429	33.05
18.1	553	16.47	3	16.59	429	33.03
18.8	553	16.46	3	16.58	429	33.02
20.1	554	16.45	2	16.53	428	32.97
21.5	554	16.42	2	16.50	428	32.94
25.5	555	16.36	1	16.40	427	32.84
29.5	556	16.30	0	16.30	426	32.74
36.0	554	16.22	2	16.30	428	32.74
40.0	552	16.17	4	16.32	430	32.76
44.0	551	16.12	5	16.31	431	32.75
135	548	15.90	8	16.21	434	32.65
175	548	15.91	8	16.21	434	32.66
215	548	15.88	8	16.19	434	32.63
415	548	15.63	8	15.94	434	32.38
455	543	15.58	13	16.08	439	32.52
395	548	15.53	8	15.84	434	32.28
535	548	15.48	8	15.79	434	32.23
615	549	15.34	7	15.61	433	32.05
735	549	15.60	7		433	
815	549	15.46	7	15.73	433	32.17
895	549	15.24	7	15.51	433	31.95
935	549	15.23	7	15.50	433	31.94
∞	25	9.82[a]	531	30.31	957	46.75
∞	196	6.93[a]				

a. See Table I-1.

TABLE I-8. Resistivity of TLC-2 to 330°C

Corrected Time (min)	T (°C)	ρ (μΩ cm)	(330°C - T)	$\rho_{330°C}$	(982°C - T)	$\rho_{982°C}$
0.0	26.2	14.53	303.5	19.54	955.4	30.30
0.1	26.2	14.53	303.9	19.54	955.8	30.30
0.2	26.0	14.53	304.1	19.55	956.0	30.31
0.3	26.0	14.53	304.1	19.55	956.0	30.31
0.4	31.4	14.67	298.7	19.60	950.6	30.36
0.5	50.7	14.73	279.4	19.34	931.3	30.10
0.6	79.8	25.12	250.3	29.26	902.2	40.02
0.7	242.5	29.14	87.6	30.58	739.5	41.34
0.8	315.1	19.32	15.0	19.56	666.9	30.32
0.9	330.1	16.40	0.0	16.40	651.9	27.16
1.0	320.3	15.92	9.8	16.08	661.7	26.84
1.1	318.3	15.73	11.8	15.92	663.7	26.68
1.2	317.2	15.75	12.9	15.96	664.8	26.72
1.3	316.0	15.73	14.1	15.96	666.0	26.72
2.3	312.9	15.63	17.2	15.92	669.1	26.68
3.3	311.4	15.61	18.7	15.91	670.6	26.67
4.3	311.0	15.60	19.1	15.92	671.0	26.68
5.3	310.7	15.61	19.4	15.93	671.3	26.69
6.3	310.7	15.60	19.4	15.92	671.3	26.68
7.3	310.4	15.59	19.7	15.91	671.6	26.67
8.3	310.3	15.57	19.8	15.89	671.7	26.65
9.3	310.2	15.57	19.9	15.89	671.8	26.65
10.3	310.4	15.56	19.7	15.89	671.6	26.65
15.3	310.1	15.51	20.0	15.84	671.9	26.60
28.3	310.2	15.44	19.9	15.77	671.8	26.53
38.3	310.3	15.38	19.9	15.71	671.8	26.47
48.3	310.4	15.35	19.7	15.68	671.6	26.44
58.3	310.6	15.33	19.5	15.65	671.4	26.41
68.3	310.7	15.30	19.4	15.62	671.3	26.38
78.3	310.9	15.28	19.2	15.60	671.1	26.36
88.3	310.8	15.26	19.3	15.58	671.2	26.34
98.3	310.8	15.24	19.3	15.56	671.2	26.32
158.3	310.3	15.16	19.8	15.48	671.7	26.24
208.3	310.4	15.11	19.7	15.44	671.6	26.20
258.3	310.7	15.08	19.4	15.40	671.3	26.16
308.3	310.6	15.05	19.5	15.37	671.4	26.13
358.3	310.6	15.02	19.5	15.34	671.4	26.10
408.3	310.5	14.99	19.6	15.31	671.5	26.07
458.3	310.5	14.98	19.6	15.30	671.5	26.06
508.3	310.7	14.96	19.4	15.28	671.3	26.04
558.3	311.1	14.96	19.1	15.27	671.0	26.03
608.3	311.1	14.92	19.0	15.23	670.9	25.99
758.3	311.1	14.92	19.6	15.23	670.9	25.99
708.3	311.1	14.89	19.0	15.20	670.9	25.96
758.3	311.4	14.87	18.7	15.18	670.6	25.94
808.3	311.2	14.86	18.9	15.18	670.8	25.94
858.3	311.1	14.85	19.0	15.16	670.9	25.92
908.3	311.2	14.84	18.9	15.15	670.8	25.91
958.3	310.8	14.80	19.3	15.11	671.2	25.87
1008.3	310.9	14.79	19.3	15.11	671.2	25.87
1058.3	310.9	14.79	19.2	15.11	671.1	25.87
∞	25.0	4.2[a]				
∞	196	1.26[a]				

a. See Table I-1.

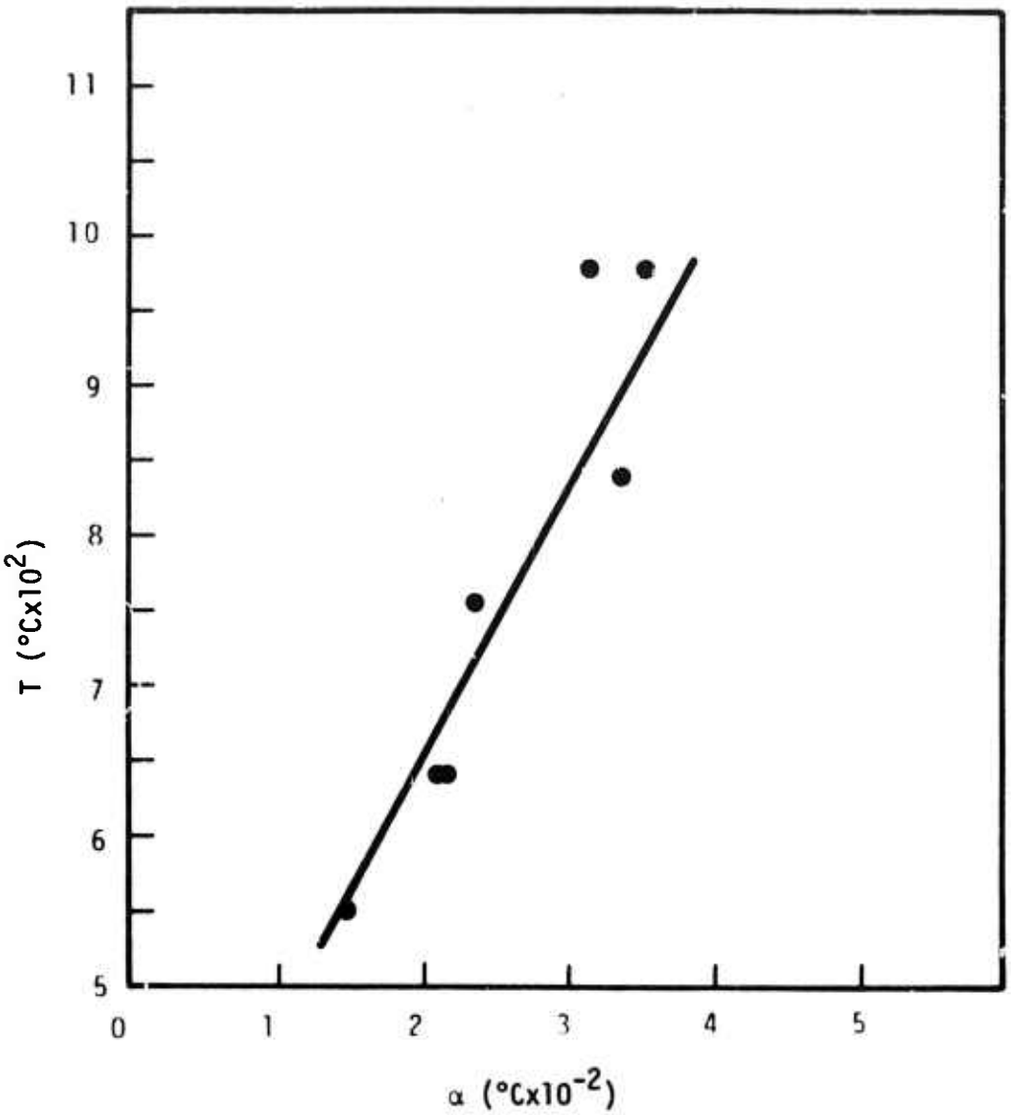

FIGURE I-1. Effect of Temperature (T) on Temperature Coefficient of Resistance (α)

REFERENCES

I-1 J. K. Stanley, Electrical and Magnetic Properties of Metals, (ASM, Metals Park, Ohio, 1963), Chapter 2.

I-2 J. H. Dellinger, The Temperature Coefficient of Resistance of Copper, Nat. Bur. Std. (US) Tech. Memc. Bull., 1, 72 (1910).

I-3 F. W. Reynolds and G. R. Stilwell, Phys. Rev. 88, 418 (1952).

I-4 K. Fuchs, Proc. Cambridge Phil, Soc., 34, 100 (1938).

I-5 A. F. Mayades and M. Shatzkes, Phys. Rev. B, 1, 1382 (1970).

I-6 E. E. Mola and J. M. Heras, Thin Solid Films, 18, 137 (1973).

APPENDIX II

DETERMINATION OF ACTIVATION ENERGIES

With the qualifications regarding temperature corrections to resistivity data discussed in Appendix I, determinations of $R = \Delta\rho/\Delta t$ were made from data shown in Tables I-1 to I-8 of Appendix I. Constant ρ (corrected to 982°C) was taken, as a first approximation, to indicate constant structure. Therefore, values of $\rho_{982°C}$ were chosen, the times to reach these corrected resistivities were noted for each resistivity experiment, and the corresponding measured resistivities (at the experiment temperatures) were recorded. This gave a measured resistivity and time at each experiment temperature for each chosen value of $\rho_{982°C}$. Values of $\Delta\rho/\Delta t$ were then calculated in the vicinity of each of these measured resistivity values from resistivity versus time data recorded at each experimental temperature. Results are presented graphically in Figures II-1, II-2, and II-3. Arrhenius analysis of these graphs yielded the activation energies also indicated in each of these figures (an approximate least-squares method was used for slope determination).

Figure II-1 indicates an activation energy of 9.63 kcal/mole for the early stages of annealing at all temperatures for structures corresponding to $\rho_{982°C}$ = 40 μΩ-cm.

If the data from 550°C are discarded or if only the resistivities during the first few seconds at 550°C are used, then the curves for structures corresponding to $\rho_{982°C}$ = 35, 33, 30, 28 μΩ-cm indicate an activation energy of 14.21 to 22.06 kcal/mole, in good agreement with the results obtained from hardness data. The neglect of the 550°C data can be justified since the laminate structure did not break up at 550°C and, further, resistivity change virtually ceased after 0.7 min at 550°C. In addition, since early data taken at 550°C falls on the curves for structures corresponding to $\rho_{982°C}$ = 40, and 35 μΩ-cm, it is hypothesized that the

resistivity changes at 550°C are probably due to recovery processes and are produced by the same mechanisms responsible for the early resistivity changes at higher temperatures.

The same arguments can be applied to 640°C resistivity data with respect to curves for structures corresponding to $\rho_{982°C}$ = 25, 24, 22 μΩ-cm in Figure II-2. If the 640°C data are neglected in these curves, the calculated activation energies are 10.18 to 11.33 kcal/mole. If these 640°C data are not neglected, however, activation energies appropriate to the third stage of structural change (+50 kcal/mole) are observed.

All of the data represented by the curves for structures corresponding to $\rho_{982°C}$ = 20, 17, 16 μΩ-cm were taken after the sample resistivities ceased to change rapidly, Figure II-3. Further, TEM results presented earlier indicated that all of these structures were spheroidized. It is likely, therefore, that the calculated activation energy from the curve for $\rho_{982°C}$ = 20 μΩ-cm of 69.85 kcal/mole is typical of the sphere coarsening mechanism while an activation energy of 10 to 22 kcal/mole is typical of the layer breakdown (spheroidization) mechanism and an activation energy of 9.6 kcal/mole (0.42 eV) is typical of the earliest annealing stage. No evidence was found to clearly indicate that the earliest annealing stage was not actually the onset of layer breakdown by Mo spheroidization.

The curve for $\rho_{982°C}$ = 17, 16 μΩ-cm indicate virtually no change in rate with temperature (above 750°C) and no activation energy. This is probably because sphere size and spacing is becoming large enough compared to the electron mean free path that small changes in sphere size and spacing do not have a sufficiently large effect on resistivity to be measurable.

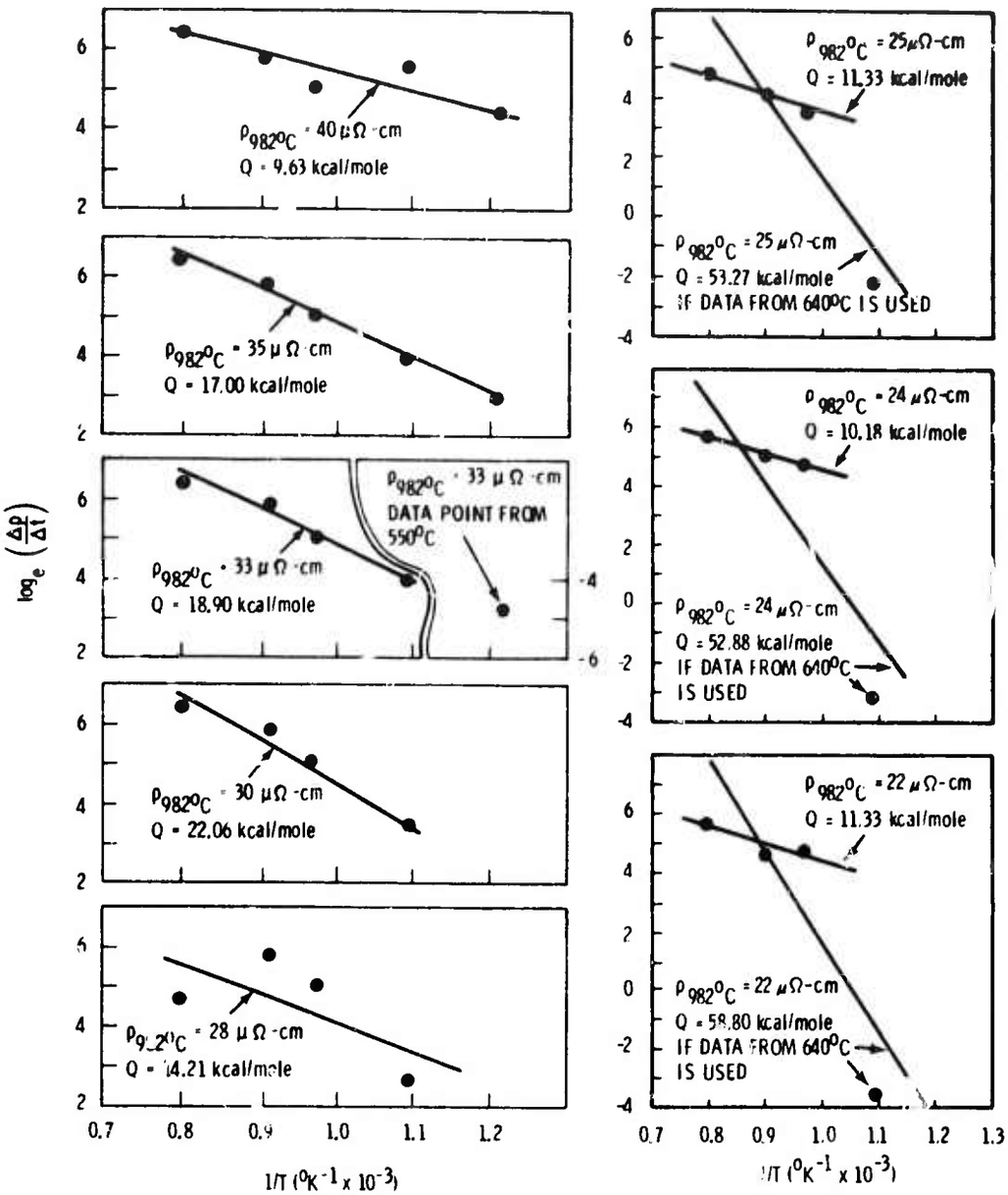

FIGURES II-1 and II-2. Arrhenius Determination of Activation Energy (Q) from Temperature (T) Dependence of the Time-Rate-of-Change of Resistivity ($\Delta\rho/\Delta t$). Constant structure was chosen corresponding to values of $\rho_{982°C}$ indicated.

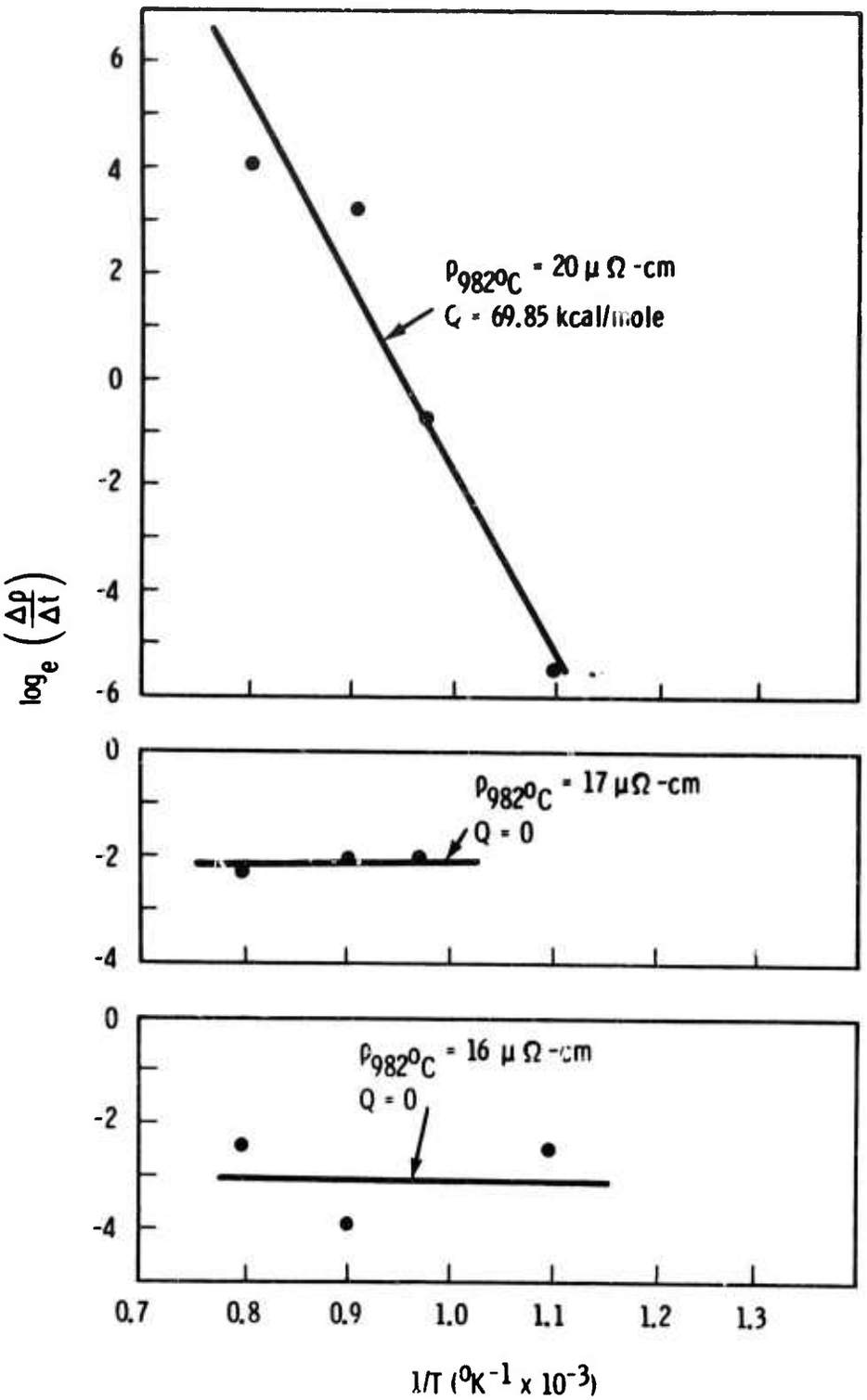

FIGURE II-3. Arrhenius Determination of Activation Energy (Q) from Temperature (T) Dependence of the Time-Rate-of-Change of Resistivity ($\Delta\rho/\Delta t$). Constant structure was chosen corresponding to values of $\rho_{982°C}$ indicated.

APPENDIX III

SUMMARY OF LITERATURE SEARCH ON ACTIVATION ENERGY DATA AND DERIVED MECHANISTIC CONSIDERATIONS

An extensive literature search revealed no previous activation energy measurements related to diffusion in the Cu-Mo system. The only pertinent data available in the published literature for comparison, then, are data obtained from self-diffusion, creep, radiation damage, and related experiments in pure Cu and Mo and data on diffusion in other fcc-bcc systems. The literature, therefore, was searched for these types of data and the results were used to interpret observed activation energies.

Since very high concentrations of vacancies, divacancies, and related defects would be expected to be quenched into high-rate sputtered materials, the thermally activated motion of these defects may have been responsible for the observed activation energies. The 9.63 kcal/mole activation energy for the first annealing stage in the present work is lower than the 15.4 kcal/mole reported for divacancy migration in Cu or the 14.2 kcal/mole for divacancy migration minus divacancy binding in Cu.[III-1,2] However, the activation energy for vacancy formation in copper is reported to be 12 to 21 kcal/mole[III-3,4,5] and the activation energy for vacancy migration is reported to be 27 to 31 kcal/mole.[III-3,4,5] Therefore, migration of vacancies to sinks should have an activation energy of 6 to 19 kcal/mole. Based on this observation, the high expected vacancy density, and the high density and close spacing of sinks (interfaces and grain boundaries) in the sputter-deposited composite, it is considered most probable that vacancy migration to sinks was responsible for the initial resistivity decrease stage. The first stage may actually have been responsible for the onset of layer breakdown by Mo spheroidization.

From the preceding comments it is apparent that the activation energy of 10 to 22 kcal/mole attributed to layer breakdown is appropriate either to vacancy migration to sinks or to vacancy migration. The latter is

considered to be the most likely of these two mechanisms. However, TEM observations reported in this report indicate that layer breakdown (spheroidization) occurs at least in part by Cu and Mo diffusion perpendicular to the layer planes. Thus the layer breakdown process may involve activation energies for diffusion of Cu or Mo vacancy species along Cu-Mo interfaces, Cu and/or Mo grain boundaries, and columnar growth boundaries. None of these activation energies have been evaluated separately. The activation energy for lattice self-diffusion in Ag is reported to be 45 kcal/mole[III-6] effectively ruling out this mechanism. Grain boundary diffusion, however, is reported to have an activation energy of 21.5 kcal/mole in Ag.[III-7] Thus the grain boundary or interface activation energies in the Cu-Mo composite of about 20 kcal/mole that would be expected were observed.

Sphere coarsening, on the other hand, must be due to Mo diffusion through the Cu matrix or to Mo sphere coalescence. One possible mechanism of Mo sphere coalescence might involve Cu vacancy diffusion to the Mo sphere, around its surface to the opposite side, and away. Motion of the Mo sphere, then, would be opposite to the flow of Cu vacancies. This would allow Mo spheres to approach each other and coalesce. Another possible mechanism for coalescence might involve diffusion of Mo around the sphere circumferences or through the spheres (self-diffusion) to produce sphere movement. Still another mechanism might involve Cu diffusion through the Mo spheres. The activation energy attributed to the sphere coarsening process is similar to the 61 to 88 kcal/mole reported for creep in Mo.[III-8] However, Claner[III-9] has reported an activation energy of 106 kcal/mole for creep in Mo and Murray[III-10] has reported an activation energy of 94 kcal/mole for self-diffusion in Mo. The activation energy for self-diffusion in Mo that is calculated by the method of Sherby and Simnad[III-11] is 98.5 kcal/mole. Vacancy migration in Mo is reported to produce an internal friction peak at 1050°C and results from recrystallization starting near 700°C with an activation energy of 34.5 to 55.2 kcal/mole,[III-12] which is too low to account for the observed value for sphere coarsening. Further, no activation energies centered about the 28.8 kcal/mole reported for recovery of irradiated Mo[III-13] or the 23 to 47 kcal/mole reported for self-diffusion

and creep in Cu[III-14-19] were observed. Peart[III-20] reported an activation energy of 100 kcal/mole for grain boundary diffusion of ^{60}Co in Mo in temperature ranges where Co would be expected to be fcc. This is higher than the observed activation energies, indicating that sphere coalescence by diffusion of Cu through the Mo spheres would not be likely.

It is tentatively concluded, therefore, that the observed activation energies for spheroidization and coarsening, 10.18 to 22.06 and 69.85 kcal/mole respectively, could have been produced by Cu-Mo boundary diffusion or Mo diffusion in Cu in these structures. This conclusion may also be supported by the tabulation of data for diffusion in Ag by Lazarus.[III-21] A large number of diffusing species were listed, and all had activation energies of less than 46 kcal/mole except Ru. Ru was the only bcc material listed and the activation energy for Ru diffusion was 65.8 kcal/mole. No other examples of diffusion of a bcc metal in an fcc lattice (except Fe) were encountered in the literature. Furthermore a recent comprehensive review of grain boundary diffusion by Gleiter and Chalmers[III-22] indicates that activation energies for Cu-Mo interface or grain boundary diffusion cannot be predicted accurately within the present state-of-the-art.

REFERENCES

III-1. D. Bowen, R. R. Eggleston and R. H. Kropschot, J. App. Phys., 23, 630 (1952).

III-2. A. Seeger, V. Gerold, K. P. Chik and M. Rühle, Phys. Letters, 5, 107 (1963).

III-3. J. A. Brinkman, C. E. Dixon and C. J. Meechan, Acta. Met., 2, 38 (1954).

III-4. S. D. Gertstriken, Dokl. Akad. SSSR, 98, 211 (1954).

III-5. C. J. Meechan and R. R. Eggleston, Acta. Met., 2, 680 (1954).

III-6. R. E. Hoffmann and D. Turnbull, J. Appl. Phys., 22, 634 (1951).

III-7. L. Slifkin, D. Lazarus and T. Tomizuka, J. Appl. Phys., 22, 1032 (1952).

III-8. H. Carvalhinhos and B. B. Argent, J. Inst. Metals, 95, 364 (1967).

III-9. A. H. Claner, Trans. Am. Soc. Metals, 61, 701 (1968).

III-10. M. J. Murray, J. of the Less-Common Metals, 15, 425 (1968).

III-11. O. D. Sherby and M. T. Simnad, Prediction of Atomic Mobility in Metallic Systems, DMS Report 61-1, Stanford University Department of Materials Science, Stanford, California, 1961.

III-12. H. Shultz, Lattice Defects in Quenched Metals, Academic Press, New York, 1965, edited by R. M. J. Cotterill, M. Doyama, J. J. Jackson and M. Meshii, p. 761.

III-13. D. E. Peacock and A. A. Johnson, Phil. Mag., 8, 563 (1963).

III-14. A. Kuper, H. Letaw, Jr., L. Slifkin, E. Sonder and C. T. Tomizuka, Phys. Rev., 98, 1870 (1955).

III-15. M. Pahutová, J. Cadek and P. Rys, Phil. Mag., 23, 509 (1971).

III-16. A. I. Il'inskii, L. S. Palatnik and N. P. Sapelkin, Sov. Phys.-Solid State, 5, 2134 (1974).

III-17. T. E. Tietz and J. E. Dorn, Trans. AIME, 156 (Feb. 1956).

III-18. J. Rogan and J. M. Alexander, J. Inst. Metals, 94, 61 (1966).

III-19. P. Feltham and J. D. Meakin, Acta. Met., 7, 614 (1959).

REFERENCES (contd)

III-20. R. F. Peart, D. Grahm and D. H. Tomlin, Acta. Met., 10, 519 (1962).

III-21. D. Lazarus, Solid State Physics, Academic Press, Inc., New York, 1960, edited by Seitz and Turnbull, Vol. 10, p. 71.

III-22. H. Gleiter and B. Chalmers, High-Angle Grain Boundaries, in Progress in Materials Science, Pergamon Press, New York, 1972, edited by B. Chalmers, J. W. Christian and T. B. Massalski, Vol. 16, Chapter 4.